The Astrophysical Journal, 952:87 (16pp), 2023 July 20 https://doi.org/10.3847/1538-4357/acd446

Relativistic Corrections in White Dwarf Asteroseismology

S. Reece Boston, Charles R. Evans, and J. Christopher Clemens
University of North Carolina, 120 E. Cameron Ave., Chapel Hill, NC 27599, USA; rboston@live.unc.edu
Received 2022 August 18; revised 2023 May 8; accepted 2023 May 9; published 2023 July 19

Abstract

With the precision now afforded by modern space-based photometric observations from the retired K2 and current TESS missions, the effects of general relativity (GR) may be detectable in the light curves of pulsating white dwarfs (WDs). Almost all WD models are calculated using a Newtonian description of gravity and hydrodynamics. To determine if the inclusion of GR leads to observable effects, we used idealized models of compact stars and made side-by-side comparisons of mode periods computed using a: (i) Newtonian and (ii) GR description of the equilibrium structure and nonradial pulsations. For application to WDs, it is only necessary to include the first post-Newtonian (1PN) approximation to GR. The mathematical nature of the linear nonradial pulsation problem is then qualitatively unchanged and the GR corrections can be written as extensions of the classic Dziembowski equations. As such, GR effects might easily be included in existing asteroseismology codes. The idealized stellar models are (i) 1PN relativistic polytropes and (ii) stars with a cold degenerate electron equation of state featuring a near-surface chemical transition from $\mu_e = 2$ to $\mu_e = 1$, simulating a surface hydrogen layer. A comparison of Newtonian and 1PN normal mode periods reveals fractional differences in the order of the surface gravitational redshift z. For a typical WD, this fractional difference is $\sim 10^{-4}$ and is greater than the period uncertainty σ_Π/Π of many WD pulsation modes observed by TESS. Consistent theoretical modeling of periods observed in these stars should, in principle, include GR effects to 1PN order.

Unified Astronomy Thesaurus concepts: Asteroseismology (73); Gravitation (661); General relativity (641); White dwarf stars (1799)

1. Introduction

Properly speaking, all stellar interiors are general relativistic because all stars self-gravitate. The question is never if general relativity (GR) applies to a stellar model, but how best to apply it.

With the exception of neutron stars, the full theory of GR is not usually necessary for describing the equilibrium or dynamics of stars, and the Newtonian approximation to gravity suffices. One caveat to this rule is that it has long been known (Harrison et al. 1965) that GR lowers the threshold for instability to radial collapse in compact stars at a local peak of a mass–radius relation. For massive white dwarfs (WDs), this affects the exact value of the (idealized) Chandrasekhar mass M_C. Relativistic polytropes provide a simple model for this effect of GR, where for a star of mass M and radius R the critical polytropic index n_c for the onset of instability is shifted (Shapiro & Teukolsky 1983) according to

$$\gamma_c = 1 + \frac{1}{n_c} = \frac{4}{3} + 2.25\,\frac{GM}{c^2 R}. \tag{1}$$

The perturbation in critical exponent γ_c is clearly proportional to the surface gravitational redshift $z = GM/(c^2R)$, which serves as a post-Newtonian (PN) compactness parameter. Recently, the effects of GR on ultra-massive WDs have been considered (Mathew & Nandy 2017; Carvalho et al. 2018; Nunes et al. 2021; Althaus et al. 2022). GR effects on the internal structure become more significant as M approaches M_C, the stellar radius shrinks, and the compactness parameter grows.

This paper is concerned with a different role played by GR, namely its effects on nonradial gravity mode (g-mode) pulsations observed in ZZ Ceti and other variable WD stars. It is reasonable to expect (which we confirm) that GR effects will show up at first order in the PN parameter (1PN) in the conservative dynamics of g-modes. While some variable WDs have higher mass, typical ZZ Ceti stars have $M \simeq 0.6 M_\odot$. These stars have surface redshifts of order $z \simeq 10^{-4}$, leading to expected fractional shifts in g-mode periods at this level. While these effects are obviously subtle, modern space-based photometry using TESS and K2 data, with long-duration observations, yields fractional uncertainties in measuring g-mode periods down to 10^{-4} or better. Some variables display modes (usually with periods in the range $\Pi \sim 100$–200 s) that are coherent over lengths of time exceeding the spacecraft observations (see Hermes et al. 2017, 2013). Even longer-duration time series, which include decades of ground-based observations, have revealed stars such as G117-B15A (Kepler et al. 2021) and R458 (Mukadam et al. 2013) with stable modes that have fractional period precisions better than $\sigma_\Pi/\Pi \sim 10^{-8}$, allowing attempts to measure WD cooling.

Recent WD asteroseismology work (Giammichele et al. 2018) has attempted to build WD models that reproduce observed pulsation periods to the level of precision of space-based data. Based on the results of our calculations comparing Newtonian and 1PN GR models, we argue that GR effects might sensibly be taken into account when trying to reproduce pulsation spectra with fractional line widths narrower than 10^{-4}.

The methods of asteroseismology (for main-sequence stars as well as WDs) have been reviewed in multiple settings (e.g., Cox 1980; Hansen & Kawaler 1994; Unno et al. 1979). The

Newtonian equations describing nonradial stellar pulsations are usually cast into a form due to Dziembowski (1971), which introduces dimensionless variables and takes account of regular singular points in the system of equations at the stellar center (origin) and surface. For example uses of these equations, see Townsend & Teitler (2013), Takata & Löffler (2004), and Córsico & Benvenuto (2002). Several community codes are available that calculate eigenmodes and periods once a stellar background model is specified. These codes include `gyre` (by Townsend & Teitler 2013) and `adipls` (by Christensen-Dalsgaard 2008), which can be incorporated in stellar evolution codes, such as `MESA` (by Paxton et al. 2010).

The theory of stellar pulsations in GR developed largely separately and was focused on the possibility of pulsations in neutron stars (Thorne & Campolattaro 1967; Price & Thorne 1969; Thorne 1969a, 1969b; Campolattaro & Thorne 1970; Ipser & Thorne 1973). For quadrupole or higher order ($\ell \geqslant 2$) nonradial modes, the gravitational field is dynamical and results in the emission of gravitational waves (GWs). The computed modes in these cases are quasi-normal with complex eigenfrequencies that reflect damping. Later work (Lindblom & Detweiler 1983; Detweiler & Lindblom 1985) simplified the system of perturbation equations to a fourth-order complex set, providing a means to more easily calculate modes numerically.

It is not necessary to apply the full machinery of GR pulsation theory to WDs. When pulsations of stars that are less compact than neutron stars are considered, like WDs, the conditions for applicability of both the slow-motion and weak-field approximations prevail, which means that the PN formalism can be used. Applied to typical WDs, where the compactness parameter is $\sim 10^{-4}$, fractional corrections to mode periods will be of this order. Even if 1PN corrections can be observed, 2PN is almost certainly unobservable. Accordingly, we propose using the 1PN approximation as an accurate means of including GR effects in WD pulsation calculations (Boston 2022) and have built an asteroseismology code, `GRPulse`, based on this premise. For consistency, 1PN GR would need to be included in both the pulsation equations and in the background stellar model.

It might be argued that the effects of GWs, which set in at 2.5PN order in the fluid motion, should be considered since they exhibit a secular behavior. However, most of the observed WD g-modes are thought to be $\ell = 1$ oscillations, which do not radiate GWs. In those modes that do radiate, the secular effect would primarily manifest itself in the mode amplitude, and be much more difficult to measure accurately than mode periods. Moreover, the Q due to GW damping of an otherwise undisturbed free WD oscillation is enormous. The coarsest approximation for the quadrupole f-mode would be $Q \sim (Rc^2/GM)^{5/2} \sim 10^{10}$. Additionally, for g-modes, the Q due to GW emission would be orders of magnitude larger still, since g-modes are primarily a motion near the surface with less mass involved in the perturbation $\Delta\rho$ and (importantly) the periods, set by the Brunt–Väisälä frequency, are much longer than those of the f-mode or p-modes. In any event, the observed sustained g-modes in WDs are not likely free oscillations but instead modes that are driven by the conversion of heat flux from the stellar interior into mechanical work, in the region of partial hydrogen ionization, by the trapping effects of the convection zone (Dolez & Vauclair 1981; Winget et al. 1982; Brickhill 1991; Goldreich & Wu 1999) and damped by the onset of dissipative mode coupling parametric instability (Wu & Goldreich 2001). These stronger effects preclude the need to consider weaker GWs (which only apply to $\ell \geqslant 2$ pulsations), and our proposed use of the 1PN approximation automatically avoids the issue.

The 1PN gravitational field involves (i) a correction to the Newtonian potential Φ, (ii) an introduction of the gravitomagnetic vector potential $\boldsymbol{W}$ (with only two nontrivial components, $\boldsymbol{W}^r$ and $\boldsymbol{W}^\theta$, in the case of fluid stars), and (iii) the presence of a new (1PN) scalar potential Ψ. Besides adding new (elliptic) field equations for these variables, numerous 1PN correction terms appear in the fluid equations of motion. As we show, in this format the usual linear pulsation equations can be extended in a transparent way.

Stellar pulsations at 1PN order have been considered previously (Cutler 1991), though in that paper applied to rotating neutron stars where the unperturbed stationary model is axisymmetric, not spherically symmetric. In Newtonian terms, the rotational (centrifugal) potential is great enough to make the background model oblate. We do not consider the complication of rapid rotation here.

Nevertheless, it is worth remembering that some pulsating WDs do exhibit the effects of rotation. Retaining only first power in the stellar angular velocity Ω (i.e., small rotation rate), the combined effects of the angular rate between the star and distant inertial observer and of the Coriolis accelerations $\boldsymbol{\Omega} \times \boldsymbol{\delta v}$ in the fluid motion lead to a splitting of circular-mode periods proportional to their value of azimuthal mode number m (Cox 1980). These splittings are observed in the power spectra of WD light curves, with groupings of $2\ell + 1$ modes (e.g., triplets for $\ell = 1$) allowing the mode number ℓ to be determined. See Kepler et al. (1983) for an observed rotational splitting of $\ell = 1$ in G226-29 and Odonoghue & Warner (1982) for the splitting of $\ell = 2$ and $\ell = 1$ in L19-2. Second-order-in-Ω effects of rotation on mode splittings are suggested by analysis of L19-2 (Odonoghue & Warner 1982; Brassard et al. 1989). Our calculations will be relevant for small rotation rates and when applied to the $m = 0$ modes.

We note in passing that other approximations in mode calculations are sometimes made. The most common is the Cowling approximation (Cowling 1941) in which the Eulerian perturbation in the gravitational potential is neglected. One historical virtue of the Cowling approximation is it showed that the resulting second-order pulsation equations could be cast in nearly Sturm–Liouville form, and in the mode frequency limits $\omega \to \infty$ or $\omega \to 0$ the system assumes Sturm–Liouville form. Out of this emerged the understanding of the existence of infinite sequences of p-modes and g-modes, separated by the single (for $\ell \geqslant 2$) f-mode. While the Cowling approximation of mode periods can be sufficiently accurate for some purposes, in this paper we seek to make an unambiguous comparison between Newtonian and 1PN GR versions of pulsation theory, and therefore avoid the additional uncertainty associated with the neglect of Eulerian gravitational perturbations.

In any event, while neglecting $\Delta\Phi$ in the Newtonian system is straightforward enough, to include the Cowling approximation in our comparison would require a 1PN version. While a form of the Cowling approximation for the full GR pulsation theory has been developed by McDermott et al. (1983; see also McDermott et al. 1985; Lindblom & Splinter 1990; Yoshida & Lee 2002), the question arises of what parts of the metric perturbation to include and what to ignore (Finn 1988). An

advantage of the approximation is that it eliminates the radiative degree of freedom (thereby eliminating GWs), yet this is true also when we adopt the 1PN system.

We note also that Finn has developed (Finn 1986, 1987) a slow-motion but not weak-field approximation for treating relativistic g-modes in neutron stars. In our application to WDs, there is no need to try to retain the complexity of a strong field treatment.

To make a comparison between Newtonian and 1PN GR pulsations, we opt for simplified treatments of the background stellar model and adiabatic fluctuations in the perturbation equations. We adopt two models for the star. The first model treats the WD as a polytrope, with a particular choice of how to extend the Newtonian polytrope to GR. By picking an adiabatic index Γ_1 that is greater than the polytropic structural exponent $\gamma = 1 + 1/n$, the model supports g-mode oscillations. While this affords a clean comparison, it has the disadvantage that g-modes in this model penetrate more deeply into the star, and the resulting periods are much shorter than observed modes. Accordingly, we have also generated a second model for the WD, in which the equation of state is just that of a cold degenerate electron gas, but one in which μ_e shifts smoothly from $\mu_e = 2$ in the core to $\mu_e = 1$ in a surface layer. This mimics the behavior of a surface hydrogen layer in a real WD. In this model, the g-mode cavity is confined near the surface, and the mode periods more nearly approximate those seen in real variable WDs. Neither of these stellar models is intended to be an accurate depiction of a real WD. Instead, our goal is to keep the microphysical description simple in order to better highlight the differences in mode periods that occur depending upon whether we use a Newtonian or a 1PN GR treatment.

This paper is organized as follows. In Section 2 we briefly review the standard Newtonian pulsation theory to set the notation. In addition to Newtonian polytropes, we describe in Section 2.4 the stratified $T = 0$ degenerate electron gas model that imitates a surface hydrogen layer. In Section 3 we summarize the 1PN formalism and introduce the linear wave equations at 1PN order. This section also discusses (Section 3.3) our particular choice for relativistic polytropes and their 1PN reduction, and (Section 3.5) the 1PN extension of our stratified $T = 0$ models. In Section 4 we reduce the Newtonian and 1PN perturbation equations into a form more suitable for numerical study, which in the Newtonian case is due to Dziembowski (1971). Tests of the numerical behavior of our two versions of the code are summarized in Section 5. We make use, in particular, of tabulated periods of polytropes (Cutler & Lindblom 1992; Lindblom et al. 1997) as code checks and, in turn, provide an expanded list for future reference. Section 5 discusses the numerical performance of the code, which is designed to be more than adequate to accurately capture $\sim 10^{-4}$ fractional differences between Newtonian and 1PN mode periods. Section 6 gives our calculated numerical period shifts for both polytropic stars and the stratified models.

2. Newtonian Nonradial Pulsations

For the sake of comparison to the 1PN equations, we summarize linear adiabatic pulsations in Newtonian stars. A fuller discussion is available in Cox (1980) and Unno et al. (1979).

2.1. Newtonian Stellar Dynamics

Consider a star with density $\rho(t, \boldsymbol{r})$, pressure $P(t, \boldsymbol{r})$, and Newtonian gravitational potential $\Phi(t, \boldsymbol{r})$. The fluid motions inside the star are described by

$$\nabla^2\Phi = 4\pi G\rho, \tag{2a}$$

$$\partial_t\rho + \nabla\cdot(\rho\boldsymbol{v}) = 0, \tag{2b}$$

$$\partial_t(\rho\boldsymbol{v}) + \nabla\cdot(\rho\boldsymbol{v}\boldsymbol{v}) = -\nabla P - \rho\nabla\Phi. \tag{2c}$$

Here Equation (2b) is the familiar continuity equation, and Equation (2c) is Newton's Second Law for a fluid under self-gravity. In the static spherically symmetric limit, Equation (2c) becomes the equation of hydrostatic equilibrium:

$$0 = \frac{dP}{dr} + \rho\frac{d\Phi}{dr}. \tag{3}$$

2.2. Newtonian Polytropes

We consider a simple model of a static star governed by a polytropic equation of state:

$$P = K\rho^{1+\frac{1}{n}}, \tag{4}$$

where n is the polytropic index. When using this simple equation of state for a static, spherical star, Equation (2) reduces to the Lane–Emden Equation (Lane 1870):

$$\frac{1}{s^2}\frac{d}{ds}\left(s^2\frac{d\theta}{ds}\right) = -\theta^n, \tag{5}$$

where the Lane–Emden solution θ is related to the density and pressure by

$$\rho(r) = \rho_c\theta(s)^n, \qquad P(r) = P_c\theta(s)^{n+1}. \tag{6}$$

The dimensionless radial variable s is defined by[1]

$$r = s\sqrt{\frac{(n+1)P_c}{4\pi G\rho_c^2}}. \tag{7}$$

See, e.g., Chandrasekhar (1939).

2.3. The Linearly Perturbed Newtonian Equations

If an element of fluid is displaced by $\delta\boldsymbol{r} = \xi(t, \boldsymbol{r})$, then the density, pressure, and Newtonian potential will be perturbed in response.[2] The unperturbed background star is described by a solution to Equations (3) and (2). For such a background, Equation (2), perturbed to first order, becomes

$$\nabla^2\Delta\Phi = 4\pi G\Delta\rho \tag{8a}$$

$$\Delta\rho = -\nabla\cdot(\rho\xi) \tag{8b}$$

$$\rho\frac{\partial^2\xi}{\partial t^2} = -\nabla\Delta P - \Delta\rho\nabla\Phi - \rho\nabla\Delta\Phi. \tag{8c}$$

These equations define a fourth-order system for the nonradial perturbations.

[1] In the Lane–Emden equation we use s and not the common ξ to avoid confusion with $\delta\boldsymbol{r} = \xi$.

[2] Throughout, we denote the Lagrange perturbations by δ and Euler perturbations by Δ. This is the opposite convention used in the GR literature, e.g., Shapiro & Teukolsky (1983). Our notation is a compromise with the Newtonian literature.

In spherical stars, the normal modes can be decomposed into spherical harmonics. Scalar perturbations become, e.g.,

$$\Delta\rho(t, \boldsymbol{r}) = \Delta\rho(r)_{\ell m} e^{i\omega t} Y_{\ell m}(\theta, \phi). \tag{9}$$

The displacement vector ξ is decomposed into a radial and a transverse vector spherical harmonic $\boldsymbol{Y}_{\ell m} = \boldsymbol{r}\nabla \boldsymbol{Y}_{\ell m}$, (see Barrera et al. 1985), so that

$$\xi(t, \boldsymbol{r}) = \xi^r_{\ell m}(r)\hat{\boldsymbol{r}} Y_{\ell m} e^{i\omega t} + \xi^H_{\ell m}(r)\boldsymbol{Y}_{\ell m} e^{i\omega t}. \tag{10}$$

When broken up in this way, Equation (8), describing the displacement, can be written in component form:

$$\frac{d\xi^r}{dr} = \left[\frac{g}{v_s^2} - \frac{2}{r}\right]\xi^r + \left[\frac{\ell(\ell+1)}{r^2\omega^2} - \frac{1}{v_s^2}\right]\chi + \frac{1}{v_s^2}\Delta\Phi, \tag{11a}$$

$$\frac{d\chi}{dr} = [\omega^2 - N^2]\xi^r + \frac{N^2}{g}\chi - \frac{N^2}{g}\Delta\Phi, \tag{11b}$$

where $\chi = r\omega^2\xi^H$ and we suppress the ℓ, m indices on the perturbed quantities, and where $v_s = \sqrt{(\partial P/\partial\rho)_{\rm ad}}$ is the local sound speed.

The quantity N appearing in Equation (11) is the Brunt–Väisälä frequency, which, along with the Lamb frequency (Cox 1980), is important for classifying regions of mode stability. The g-modes are restored by buoyancy forces, and cannot propagate within convective regions in the star. Stability against convection and propagation of g-modes depends on N^2 being positive (see, e.g., Kawaler et al. 1985). The Brunt–Väisälä frequency is closely related to the Schwarzschild discriminant:

$$A = \frac{d\ln\rho}{dr} - \frac{1}{\Gamma_1}\frac{d\ln P}{dr} = -\frac{N^2}{g}, \tag{12}$$

where g is the local gravity. Thus, the Schwarzschild discriminant satisfies $A < 0$ in regions where g-modes propagate.

In a spherically symmetric star, the g- and p-modes can be labeled by the angular momentum number ℓ (the modes are independent of the azimuthal number m in nonrotating stars), and further labeled by the principal radial mode number k counting the radial nodes in each mode. Using the Osaki–Scuflaire classification scheme (Osaki 1975; Scuflaire 1974), we can classify $k < 0$ as g-modes, $k > 0$ as p-modes, and the fundamental mode (f-mode) as $k = 0$.

2.4. Stratified Degenerate Electron Gas Models (CHWD++)

To begin building a simplified model that will mimic the pulsational behavior of WDs, we start with the Chandrasekhar WD (CHWD) equation of state, with the only pressure contribution coming from the completely degenerate ($T = 0$) electrons immersed in a sea of ions (Chandrasekhar 1939). We neglect electrostatic corrections. The CHWD models are not immediately suitable for asteroseismology since they have $N^2 = 0$ everywhere and do not admit g-mode solutions. Real variable WDs have g-modes that are confined near the surface (Winget et al. 1982). Important in explaining the presence of these near-surface modes is the addition of the Ledoux term in the Brunt–Väisälä frequency (Brassard et al. 1991), associated with composition transitions occurring in the outer layers. We can make a small adjustment to the CHWD $T = 0$ equation of state by adding a composition transition, and thereby construct simple stellar models that support g-modes.

To account for a chemical transition, we consider μ_e (the mean molecular weight per electron) defined by

$$\frac{1}{\mu_e} = \sum\frac{Z_i}{A_i}X_i, \tag{13}$$

where Z_i and A_i are the nuclear charge and nuclear mass numbers, respectively, and X_i is the (local) mass fraction of any elemental species. In the outermost layer composed of pure hydrogen, we will have $\mu_e = 1$, while $\mu_e = 2$ in any region composed only of ^{4} He, ^{12} C, ^{16} O, or combinations thereof. If an outer region exists where $X_{\rm He} + X_{\rm H} = 1$ and $X_{\rm He}$ smoothly transitions from 1 to 0, then $\mu_e(r)$ will smoothly transition from 2 to 1, yielding the desired near-surface cavity.

We take for the equation of state

$$\rho(r) = B_0\mu_e x^3, \tag{14a}$$

$$P(r) = A_0 f(x), \tag{14b}$$

with A_0 and B_0 being parameters (Hansen & Kawaler 1994) dependent upon electron and proton masses and physical constants h and c. Here, x and $f(x)$ are the dimensionless Fermi momentum and dimensionless degeneracy pressure function (Chandrasekhar 1939), respectively, and μ_e is assumed to vary spatially. To construct our stratified model, we set μ_e to be a function of pressure:

$$\mu_e(r) = 1 + \frac{1}{1 + \exp\{\alpha(\ln f_c - \ln f(x))\}}. \tag{15}$$

With appropriate choices for α and f_c, we can place the transition near the WD surface. Then, in constructing the stellar model, μ_e will begin at $\mu_e(0) = 2$ in the center and near the surface smoothly transition to $\mu_e(R) = 1$. With this simple equation of state, the equation of hydrostatic equilibrium reduces (in terms of dimensionless radius s) to

$$\frac{1}{s^2}\frac{d}{ds}\left(s^2\frac{dy}{ds}\right) = -\mu_e^2(y^2 - 1)^{3/2} + \frac{1}{\mu_e}\frac{dy}{ds}\frac{d\mu_e}{ds}, \tag{16}$$

where $y = \sqrt{x^2 - 1}$ and $s = rB_0\sqrt{\pi G/2A_0}$. Following Brassard et al. (1991), we can choose μ_e as the unique indicator of composition change, and it can be shown that N^2 becomes

$$N^2 = -g\frac{d\ln\mu_e}{dr}. \tag{17}$$

Thus, g-modes will exist in any region of decreasing μ_e, which we choose to be near the surface. As seen in Figure 1, this leads to a curve for N^2 that has qualitative similarities to those seen in realistic WDs. We refer to this cold degenerate but stratified model as the CHWD++ model (Boston 2022).

3. Post-Newtonian Nonradial Pulsations

Modern post-Newtonian theory, using either the multipolar post-Minkowskian (MPM) or PN approach or the direct integration of the relaxed Einstein equations formulation, has been successful in self-consistently pushing PN results to high order. See Blanchet (2014) and Poisson & Will (2014) for reviews. For example, the source motion and gravitational waves in the two-body problem have been computed to third

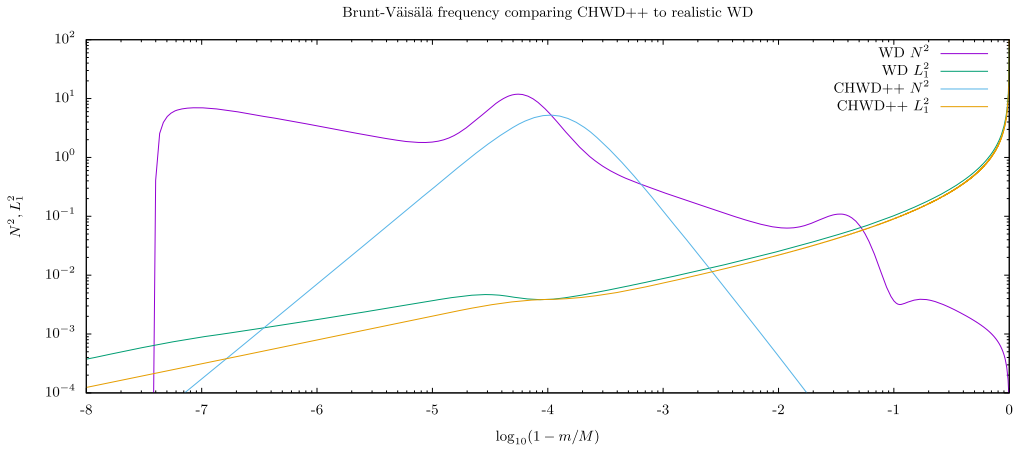

Figure 1. Comparison between the square of the Brunt–Väisälä frequency N^2 found in the CHWD++ models (blue curve) developed in this paper with N^2 that appears in realistic WD models (magenta curve) (see Boston 2022). Also plotted is the Lamb frequency L_1^2 for $\ell = 1$ (green and gold curves) to highlight the presence of the g-mode cavities, which occur in regions where the mode frequency ω satisfies both $\omega^2 < N^2$ and $\omega^2 < L_1^2$. The stellar surface is located to the left in the plot and the stellar core to the right. The presence of the composition change in the outer layers allows for a nonzero N^2 in the stratified degenerate electron model, forming a g-mode cavity qualitatively similar to those found in realistic WDs.

post-Newtonian order (Arun et al. 2008) and beyond. Our present interest in 1PN is more modest and allows the use of the simple classic approach to PN theory (Poisson & Will 2014; see their Section 8.2). We briefly summarize the formalism here.

3.1. Post-Newtonian Field Equations

Gravity arises as the result of spacetime curvature responding to the presence of matter (i.e., energy, momentum, and stress). The gravitational field is described by the metric tensor $g_{\alpha\beta}$, which determines, in part, the line element that expresses infinitesimal proper distances and times between events. At 1PN order, the line element can take the form

$$\begin{aligned} ds^2 &= g_{\alpha\beta}dx^\alpha dx^\beta \\ &= -\left(1 + \frac{2\Phi}{c^2} + \frac{2(\Psi + \Phi^2)}{c^4}\right)c^2dt^2 + \frac{8}{c^2}\vec{W}\cdot d\vec{x}\,dt \\ &\quad + \left(1 - \frac{2\Phi}{c^2}\right)[dx^2 + dy^2 + dz^2], \end{aligned} \tag{18}$$

where Φ is the usual Newtonian gravitational potential, $\boldsymbol{W}$ is a 1PN vector (gravitomagnetic) potential, and Ψ is a 1PN scalar potential. (Much of the PN literature uses $U = -\Phi$ for the gravitational potential and opposite signs on the 1PN fields. Because we make the connection with Newtonian asteroseismology, we retain the astrophysical convention for Φ and keep signs on $\boldsymbol{W}$ and Ψ consistent with that). The field is assumed to be weak, with the gravitational field spurring small deviations in the metric from that of flat space. Factors of $1/c^2$ keep track of relative PN order. The coordinates x,y,z are nearly Minkowskian, and the harmonic gauge condition

$$\partial_t\Phi + \partial_k W^k = 0 \tag{19}$$

is adopted.

The metric of Equation (18) is assumed to satisfy the Einstein field equations (see Weinberg 1972; Poisson & Will 2014),

$$G^{\alpha\beta} = \frac{8\pi G}{c^4}T^{\alpha\beta}, \tag{20}$$

term by term in the weak-field and slow-motion expansions. Here $G^{\alpha\beta}$ is the Einstein tensor, which describes spacetime curvature, and $T^{\alpha\beta}$ is the stress–energy tensor, which describes the matter. Both tensors depend on the metric $g_{\alpha\beta}$. We take the matter to be a perfect fluid described by

$$T^{\alpha\beta} = (\rho + P/c^2)u^\alpha u^\beta + P\,g^{\alpha\beta}, \tag{21}$$

with ρ the total energy density, P the isotropic pressure, and u^α the fluid 4-velocity. The 4-velocity is constrained by $u_\alpha u^\alpha = -c^2$, so that $u^\alpha = \gamma(c,\ v^k)$ with γ determined from the coordinate velocity v^k and the constraint. We further define the baryon rest mass density ρ_0 that gives rise to baryon conservation $\nabla_\alpha(\rho_0 u^\alpha) = 0$. Then, ρ and ρ_0 are related by defining the specific internal energy ε such that $\rho = \rho_0(1 + \varepsilon/c^2)$. The matter configuration is determined by a set of matter variables, such as $\{\rho,\ P,\ \varepsilon,\ v^k\}$. Alternatively, ρ_0 may be used in place of ρ. Another more common alternative is to use the conserved, or rescaled, mass density ρ^* (Poisson & Will 2014) defined by $\rho^* = \sqrt{-g}\ \gamma\rho_0$.

Using the matter set $\{\rho,\ P,\ \varepsilon,\ v^k\}$ and recalling that in the slow-motion near zone, time derivatives of functions are of order $1/c$ compared to space derivatives, the 1PN field equations become

$$\nabla^2\Phi = 4\pi G\rho, \tag{22a}$$

$$\nabla^2\boldsymbol{W} = 4\pi G\rho\boldsymbol{v}, \tag{22b}$$

$$\nabla^2\Psi = \frac{\partial^2\Phi}{\partial t^2} + 4\pi G(2\rho v^2 - 2\rho\Phi + 3P), \tag{22c}$$

where ∇^2 is the flat-space Laplacian. Leaving aside the choice of sign for the potentials, the use of ρ in the fundamental matter set, rather than ρ_0 or ρ^*, affects the form of the source in (22c) and, therefore, the definition of Ψ. The form of the 1PN field equations we list here is equivalent to that found in Weinberg (1972) but differs from that in Poisson & Will (2014). A more

detailed derivation of these equations is found in Boston (2022).

3.2. Post-Newtonian Hydrodynamics

The 1PN system is completed by deriving the 1PN equations of motion of the perfect fluid. The stress–energy tensor has vanishing covariant divergence:

$$\nabla_\alpha T^{\alpha\beta} = \partial_\alpha T^{\alpha\beta} + \Gamma^\beta_{\alpha\gamma} T^{\alpha\gamma} + \Gamma^\alpha_{\alpha\gamma} T^{\gamma\beta} = 0. \tag{23}$$

Inserting the perfect fluid stress tensor and expansions for the connection, metric determinant, and 4-velocity through 1PN order, the time component of Equation (23) is found to be

$$\frac{\partial}{\partial t}\left[\rho\left(1 + \frac{v^2 - 2\Phi}{c^2}\right)\right] + \nabla\cdot\left[\rho\boldsymbol{v}\left(1 + \frac{v^2 - 2\Phi}{c^2}\right) + \frac{P\boldsymbol{v}}{c^2}\right] - \frac{\rho}{c^2}\frac{\partial\Phi}{\partial t} = 0, \tag{24a}$$

where ∇ is the flat-space operator. The space components of Equation (23) reduce to 1PN order in a similar fashion:

$$\frac{\partial}{\partial t}\left[\rho\boldsymbol{v}\left(1 + \frac{v^2 - 4\Phi}{c^2}\right) + \frac{P\boldsymbol{v}}{c^2}\right] + \nabla\cdot\left[\rho\boldsymbol{v}\boldsymbol{v}\left(1 + \frac{v^2 - 4\Phi}{c^2}\right) + \frac{P\boldsymbol{v}\boldsymbol{v}}{c^2}\right] + \nabla P + \rho\nabla\Phi + \frac{1}{c^2}\{\rho\nabla\Psi + (P + 2\rho v^2\nabla\Phi + \left(4\rho\frac{\partial\boldsymbol{W}}{\partial t} - 2\rho\boldsymbol{v}\frac{\partial\Phi}{\partial t} - 2\rho\boldsymbol{v}(\boldsymbol{v}\cdot\nabla\Phi) - 4\rho\boldsymbol{v}\times(\nabla\times\boldsymbol{W})\right\} = 0. \tag{24b}$$

Combining Equations (24a) and (24b) we can derive the 1PN version of Euler's equation for the time rate of change of the 3-velocity.

For a relativistic barytropic equation of state, $P = P(\rho)$ (such as the 1PN polytropes we consider below) and Equation (22) along with Equation (24) suffice to characterize the 1PN system. For a more general equation of state, where $P = P(\rho_0, \Pi)$, these equations must be supplemented with the expression for the conservation of the baryon number. In the limit, as $1/c \to 0$, everything reduces to the Newtonian system of Equation (2).

In the static limit for a spherical configuration, Equation (24b) reduces to

$$\frac{dP}{dr} + (\rho + P/c^2)\frac{d\Phi}{dr} + \frac{\rho}{c^2}\frac{d\Psi}{dr} = 0, \tag{25}$$

which is the 1PN version of the Tolman–Oppenheimer–Volkoff (TOV) equation of relativistic hydrostatic equilibrium (Oppenheimer & Volkoff 1939; Tolman 1939).

3.3. 1PN Polytropes

For the case of a 1PN static spherical polytrope, we follow Tooper's (1964) solution to the equations of a static fluid sphere in GR (see also Oppenheimer & Volkoff 1939; Tolman 1939). We specify an equation of state identical in form to Equation (4), where $\rho = \epsilon/c^2$ represents the mass-energy density inside the star (and not merely the baryon density as in Tooper's 1965 paper). We define the dimensionless relativistic parameter:

$$\sigma = \frac{P_c}{\rho_c c^2}, \tag{26}$$

specifying the strength of relativity within the star. This σ can be related to the surface redshift z. In addition to θ defined by Equation (6) and s defined by Equation (7), we define ϕ and ψ such that

$$\Phi(r) = \frac{(n+1)P_c}{\rho_c}\phi(s), \tag{27a}$$

$$\Psi(r) = \frac{(n+1)P_c^2}{\rho_c^2}\psi(s). \tag{27b}$$

In the static case, Equations (22) and (24a) can be reduced to

$$\frac{1}{s^2}\frac{d}{ds}\left(s^2\frac{d\theta}{ds}\right) = -\theta^n + \sigma\left[2(n+1)\theta^n\phi - 4\theta^{n+1} - \frac{d\phi}{ds}\frac{d\theta}{ds}\right], \tag{28a}$$

$$\frac{1}{s^2}\frac{d}{ds}\left(s^2\frac{d\phi}{ds}\right) = \theta^n, \tag{28b}$$

$$\frac{1}{s^2}\frac{d}{ds}\left(s^2\frac{d\psi}{ds}\right) = 3\theta^{n+1} - 2(n+1)\theta^n\phi, \tag{28c}$$

which are 1PN Lane–Emden equations. In this form, it is clear that in the Newtonian limit $\sigma \to 0$, $\frac{d\phi}{ds} \to -\frac{d\theta}{ds}$, and Equation (28) reduce to Equation (5). From Equation (25), Equation (28b) can be replaced by

$$\frac{d\theta}{ds} = -(1 + \sigma\theta)\frac{d\phi}{ds} - \sigma\frac{d\psi}{ds}, \tag{29}$$

which is better for numerical analysis. The boundary conditions (BCs) on these equations are that $\theta = 1$ at the center, $\theta = 0$ at the surface, $d\phi/ds = d\psi/ds = 0$ at the center, and ϕ must have an initial value so that $\Phi = -GM/R$ at the surface. The value of σ must be chosen to match the redshift by

$$z = (1 - 2GM/c^2R)^{-1/2} - 1 \approx (n+1)\sigma s_1\frac{d\phi}{ds_1}, \tag{30}$$

with s_1 the value of s at the surface. This matching of $\phi(0)$, σ must be accomplished by an iterative convergence routine.

3.4. The Linearly Perturbed 1PN Equations

Consider a solution to Equation (24) for the case of a static, spherically symmetric star, and consider its response to a displacement of the fluid elements by $\delta\boldsymbol{r} = \xi$. This will result in perturbations $\Delta\rho$, ΔP, $\Delta\Phi$, $\Delta\Psi$, and $\Delta\boldsymbol{W}$. Perturbed to first order on a static background, Equation (24) will become

$$0 = \nabla\cdot\left[\xi\left(\rho + \frac{P - 2\rho\Phi}{c^2}\right)\right] + \Delta\rho\left(1 - \frac{2\Phi}{c^2}\right) - \frac{3\rho\Delta\Phi}{c^2}, \tag{31a}$$

$$0 = \left(\rho + \frac{P - 4\rho\Phi}{c^2}\right)\frac{\partial^2 \xi}{\partial t^2} + \nabla\Delta P + \rho\nabla\Delta\Phi + \Delta\rho\nabla\Phi + \frac{1}{c^2}\{\rho\nabla\Delta\Psi + \Delta\rho\nabla\Psi + P\nabla\Delta\Phi + \Delta P\nabla\Phi + 4\rho\frac{\partial\Delta \boldsymbol{W}}{\partial t}\}. \quad (31b)$$

The equations for the potentials are simply

$$\nabla^2\Delta\Phi = 4\pi G\Delta\rho, \quad (32a)$$

$$\nabla^2\Delta \boldsymbol{W} = 4\pi G\rho\partial_t\xi, \quad (32b)$$

$$\nabla^2\Delta\Psi = \partial_t^2\Delta\Phi + 4\pi G[3\Delta P - 2\rho\Delta\Phi - 2\Phi\Delta\rho]. \quad (32c)$$

On a spherical background, the scalar perturbations of the normal modes will be proportional to a spherical harmonic $Y_{\ell m}$ and have harmonic time dependence $e^{i\omega t}$, analogously to the Newtonian case. Because ξ and $\Delta \boldsymbol{W}$ are vectors, they require vector spherical harmonics,

$$\xi(\boldsymbol{r}, t) = \xi^r \hat{\boldsymbol{r}} Y_{\ell m} e^{i\omega t} + \xi^H \boldsymbol{Y}_{\ell m} e^{i\omega t}, \quad (33a)$$

$$\Delta \boldsymbol{W}(\boldsymbol{r}, t) = \Delta W^r \hat{\boldsymbol{r}} Y_{\ell m} e^{i\omega t} + \Delta W^H \boldsymbol{Y}_{\ell m} e^{i\omega t}. \quad (33b)$$

The vector Laplacian acting on $\Delta \boldsymbol{W}$ will produce two second-order equations,

$$\frac{1}{r^2}\frac{d}{dr}\left(r^2\frac{d\Delta W^r}{dr}\right) - \frac{2 + \ell(\ell+1)}{r^2}\Delta W^r + \frac{2\ell(\ell+1)}{r^2}\Delta W^H = 4\pi G\rho i\omega\xi^r, \quad (34a)$$

$$\frac{1}{r^2}\frac{d}{dr}\left(r^2\frac{d\Delta W^H}{dr}\right) - \frac{\ell(\ell+1)}{r^2}\Delta W^H + \frac{2}{r^2}\Delta W^r = 4\pi G\rho i\omega\xi^H. \quad (34b)$$

This apparent tenth-order system actually reduces to the eighth-order system of Equation (49), due to the harmonic coordinate condition of Equation (19). The perturbed version of the gauge condition is

$$0 = \partial_t\Delta\Phi + \nabla\cdot\Delta \boldsymbol{W} = i\omega\Delta\Phi(r) + \frac{1}{r^2}\frac{d}{dr}[r^2\Delta W^r(r)] - \frac{\ell(\ell+1)}{r}\Delta W^H. \quad (35)$$

This, and its derivative, allow us to eliminate two degrees of freedom from the system.

3.5. 1PN CHWD++

The 1PN generalization of the CHWD++ model introduced in Section 2.4 can be readily derived from the GR degenerate gas equation of state given by Chandrasekhar & Tooper (1964), using their functions $g(x)$ and $h(x)$, with

$$\rho(r) = \rho_B(r) + \frac{1}{c^2}U_e(r) = B_0 h(x, s) = B_0[\mu_e(s)x^3 + \sigma g(x)], \quad (36a)$$

$$P(r) = A_0 f(x), \quad (36b)$$

and with $\mu_e(x)$, as in Equation (15). Then, the static equilibrium condition of Equation (25) becomes

$$\frac{dx}{ds} = -\frac{y}{x^4}\left\{[h(x) + \sigma f(x)]\frac{d\phi}{ds} + \sigma h(x)\frac{d\psi}{ds}\right\} \quad (37a)$$

$$\frac{d}{ds}\frac{d\phi}{ds} = h(x) - \frac{2}{s}\frac{d\phi}{ds} \quad (37b)$$

$$\frac{d}{ds}\frac{d\psi}{ds} = 3f(x) - 16h(x)\phi - \frac{2}{s}\frac{d\psi}{ds}, \quad (37c)$$

where $\Phi = 8A_0/B_0\phi$ and $\Psi = 8A_0^2/B_0^2\psi$. The BCs are that $x = 0$ at the surface, that $d\phi/ds = d\psi/ds = 0$ at the center, and that ϕ must have an initial value so that $\Phi = -GM/R$ at the surface. The central value of y (and hence x) is specified by the free parameter y_0, and $\sigma = A_0/B_0c^2$ is fixed by the relative masses of protons and electrons.

4. The Dziembowski Form for Numerical Solution

We seek dimensionless forms of both Equation (8) and Equation (31) that are suitable for the numerical study of the wave equations. We choose the dimensionless form of Dziembowski (1971) for the Newtonian case, which we generalize to 1PN.

4.1. The Newtonian Dziembowski Equations

We begin with the Newtonian Equations of (8). Define variables

$$y_1 = x^{2-\ell}\frac{\xi^r(r)}{r}, \quad y_2 = x^{2-\ell}\frac{\omega^2}{g}\xi^H(r), \quad y_3 = x^{2-\ell}\frac{\Delta\Phi(r)}{gr}, \quad y_4 = x^{2-\ell}\frac{1}{g}\frac{d\Delta\Phi(r)}{dr}, \quad (38)$$

with $g = d\Phi/dr$, $x = r/R$, and the factor $x^{2-\ell}$ to improve behavior near the center. We then define a set of dimensionless stellar structure quantities:

$$A^* = \frac{1}{\Gamma_1}\frac{d\ln P}{d\ln r} - \frac{d\ln\rho}{d\ln r}, \quad V_g = -\frac{1}{\Gamma_1}\frac{d\ln P}{d\ln r}, \quad U = \frac{d\ln g}{d\ln r} + 2, \quad c_1 = \frac{GM}{R^3}\frac{r}{g}, \quad (39)$$

and define the dimensionless frequency

$$\bar{\omega}^2 = \omega^2\frac{R^3}{GM}. \quad (40)$$

The linear system describing the pulsations now becomes the Dziembowski form:

$$x\frac{dy_1}{dx} = [V_g - 3 + (2-\ell)]y_1 + \left[\frac{\ell(\ell+1)}{c_1\bar{\omega}^2} - V_g\right]y_2 + V_g y_3, \quad (41a)$$

$$x\frac{dy_2}{dx} = [c_1\bar{\omega}^2 - A^*]y_1 + [1 + A^* - U + (2-\ell)]y_2 - A^* y_3, \quad (41b)$$

$$x\frac{dy_3}{dx} = [1 - U + (2-\ell)]y_3 + y_4, \quad (41c)$$

$$x\frac{dy_4}{dx} = UA^* y_1 + UV_g y_2 + [\ell(\ell+1) - UV_g]y_3 + [(2-\ell) - U]y_4. \quad (41d)$$

Near the center, all solutions can be expanded in positive, even powers of x, and the central values satisfy

$$y_2(0) = \frac{c_1\bar{\omega}^2}{\ell} y_1(0), \qquad y_4(0) = \ell y_3(0). \tag{42a}$$

Near the surface, due to the vanishing pressure and density, the variables A^* and V_g will both diverge. Nonetheless, imposing the condition $\delta P = 0$ at the surface ($x = 1$) leads to BCs:

$$y_2(1) = y_1(1) + y_3(1), \qquad y_4(1) = -(\ell+1)y_3(1). \tag{42b}$$

While the BCs given in Equation (42) relate the boundary values, more care is needed for numerical solutions at both boundaries. For improved accuracy, we use an even-powered series at the center (see Cox 1980, Section 17.6), and follow the surface expansion approach detailed by Christensen-Dalsgaard & Mullan (1994) in their Appendix. See Boston (2022) for further details.

4.2. The 1PN Dziembowski Equations

We now consider the 1PN Equation of (31). We define variables y_1–y_4 analogously to Equation (38), but replacing

$$g \to q = \frac{d\Phi}{dr} + \frac{1}{c^2}\frac{d\Psi}{dr}. \tag{43}$$

We then define additional variables for the 1PN potentials:

$$z_1 = x^{2-\ell}\frac{\Delta\Psi}{qr\Phi_s}, \quad z_2 = x^{2-\ell}\frac{1}{q\Phi_s}\frac{d\Delta\Psi}{dr}, \tag{44}$$

and

$$z_3 = x^{2-\ell}\frac{4i\omega}{q\Phi_s}\Delta W^r, \quad z_4 = x^{2-\ell}\frac{4i\omega r}{q\Phi_s}\frac{d\Delta W^r}{dr}, \tag{45}$$

along with

$$z_5 = x^{2-\ell}\frac{4i\omega}{q\Phi_s}\Delta W^H, \quad z_6 = x^{2-\ell}\frac{4i\omega r}{q\Phi_s}\frac{d\Delta W^H}{dr}, \tag{46}$$

where $\Phi_s = -GM/R$ is the surface gravitational potential. While there are 10 variables, due to the harmonic coordinate condition only 8 of them are independent.

As in the Newtonian case of Equation (39), we define stellar quantities

$$A^* = \frac{1}{\Gamma_1}\frac{d\ln P}{d\ln r} - \frac{1}{1+P/\rho c^2}\frac{d\ln\rho}{d\ln r},$$
$$V_g = -\frac{1}{\Gamma_1}\frac{d\ln P}{d\ln r},\ U = \frac{d\ln q}{d\ln r} + 2,\ c_1 = \frac{GM}{R^3}\frac{r}{q}, \tag{47a}$$

and use $\bar{\omega}^2$, as in Equation (40). Additionally, we define

$$\Phi^* = \Phi/\Phi_s, \quad \beta_*^2 = v_s^2/\Phi_s, \tag{48}$$

where $v_s = \sqrt{(\partial P/\partial\rho)_{\rm ad}}$ is the local relativistic sound speed. To 1PN order, the surface redshift is $z = \frac{GM}{c^2R} = -\frac{\Phi_s}{c^2}$, which will be used as a relativistic PN compactness parameter.

We can eliminate z_4 and z_6 from all equations using Equation (35), which leads to an eighth-order system of equations describing 1PN pulsations:

$$x\frac{dy_1}{dx} = [V_g - 3 - 3zV_g\beta_*^2 + (2-\ell)]y_1 + \left[\frac{\ell(\ell+1)}{c_1\bar{\omega}^2} - V_g - 4zV_g\Phi^*\right] \times y_2 + [V_g - 3zV_g\beta_*^2]y_3 - zV_gz_1 - zV_gz_5, \tag{49a}$$

$$x\frac{dy_2}{dx} = \left[c_1\bar{\omega}^2 - A^* + z\left(4A^*\Phi^* - \frac{4U\bar{\omega}^2x^2}{\ell(\ell+1)}\right)\right] \times y_1 + [1 + A^* - U - 4zV_g\beta_*^2 + (2-\ell)]y_2 + [-A^* + 4zA^*\Phi^*] \times y_3 - z\left[\frac{4\bar{\omega}^2x^2}{\ell(\ell+1)}\right]y_4 + zA^*z_1 + zA^*z_5, \tag{49b}$$

$$x\frac{dy_3}{dx} = [1 - U + (2-\ell)]y_3 + y_4, \tag{49c}$$

$$x\frac{dy_4}{dx} = UA^*\left[1 + 2z\left(\frac{\beta_*^2}{\Gamma_1} - \Phi^*\right)\right] \times y_1 + UV_g\left[1 + 2z\left(\frac{\beta_*^2}{\Gamma_1} + \Phi^*\right)\right]y_2 + \left[\ell(\ell+1) - UV_g\left(1 + 2z\left[\frac{\beta_*^2}{\Gamma_1} - \Phi^*\right]\right)\right]y_3 + [(2-\ell) - U]y_4 + zUV_gz_1 + zUV_gz_5, \tag{49d}$$

$$x\frac{dz_1}{dx} = [1 - U + (2-\ell)]z_1 + z_2, \tag{49e}$$

$$x\frac{dz_2}{dx} = -2A^*U\Phi^*y_1 + [3UV_g\beta_*^2 - 2UV_g\Phi^*] \times y_2 + [2UV_g\Phi^* - 5UV_g\beta_*^2 + \bar{\omega}^2x^2]y_3 + \ell(\ell+1)z_1 + [(2-\ell) - U]z_2, \tag{49f}$$

$$x\frac{dz_3}{dx} = -4\bar{\omega}^2x^2y_3 + [(2-\ell) - U]z_3 + \ell(\ell+1)z_5, \tag{49g}$$

$$x\frac{dz_5}{dx} = \frac{4U\bar{\omega}^2x^2}{\ell(\ell+1)}y_1 + \frac{4\bar{\omega}^2x^2}{\ell(\ell+1)}y_4 + z_3 + [1 - U + (2-\ell)]z_5. \tag{49h}$$

We have derived Equation (49) in two ways: one by using the classical PN approach directly; and again using the MPM/PN approach mentioned earlier. Compare these equations to Equation (41). Notice that all new terms in these equations occur multiplied by the 1PN compactness parameter z. We therefore recover the classical Dziembowski equations in the Newtonian limit of $z \to 0$.

At the center of the star,

$$y_2(0) = \frac{c_1\bar{\omega}^2}{\ell}y_1(0), \quad y_4(0) = \ell y_3(0), \tag{50a}$$

$$z_2(0) = \ell z_1(0), \quad z_3(0) = \ell z_5(0), \tag{50b}$$

while at the surface

$$y_2(1) = [y_1(1) + y_3(1)](1 - 3z\beta_*^2 - 4z\Phi^*) - z[z_1(1) + z_5(1)], \quad (51a)$$

$$y_4(1) = -(\ell + 1)y_3(1), \quad (51b)$$

$$z_2(1) = -(\ell + 1)z_1(1), \quad (51c)$$

$$z_3(1) = -(\ell + 1)z_5(1) + \frac{4\bar{\omega}^2}{\ell}y_3(1). \quad (51d)$$

Similarly to the Newtonian problem, the solution at both the center and surface boundaries can be expanded in a power series, where the coefficients are determined only by the background model.

We draw a comparison between these 1PN terms and the Newtonian Cowling approximation. For nonradial pulsations, the full analysis should include matter perturbations, Eulerian gravitational perturbations, and thermodynamic perturbations. Often, we are most interested in the adiabatic approximation, which includes only the matter and gravitational perturbations. In the Cowling approximation, we further simplify by neglecting the Eulerian gravitational perturbations and including only matter perturbations. The adiabatic analysis can be considered to be the Cowling approximation with additional gravitational terms, and the nonadiabatic analysis can be considered to be the adiabatic approximation with additional thermodynamic terms.

In a similar way, the adiabatic 1PN effects of this paper can be considered an additional add-on to the Newtonian adiabatic approximation and can be handled similarly to the nonadiabatic effects (i.e., with numerical flags). This makes the 1PN Equation (49) easy to integrate into codes written for Newtonian analysis. This is another major benefit of the 1PN approach.

In Section 6 we will discuss the eigenfrequencies of the system of Equation (49) and compare them with the Newtonian results.

5. Numerical Tests

To ensure parity in the analysis, we produced a code to calculate eigenmodes using Newtonian and 1PN physics with polytropic backgrounds. While there are published tables for frequencies in the Newtonian case (such as Christensen-Dalsgaard & Mullan 1994, henceforth JCD–DJM) and readily available community codes (such as `gyre` and `adipls`), making our own Newtonian code grants an additional check to the 1PN frequencies that the differences are not due to method or machine.

5.1. The `GRPulse` Asteroseismology Code

Our code for both Newtonian and GR pulsations is called `GRPulse`,[3] originally introduced in Boston (2022). This code may be obtained from GitHub.[4] Documentation and sample input files to generate the tabulated values in this paper are available. The program leverages object-oriented design for easy compatibility with different stellar models, different wave equations, or different integration methods. We offer this code under the GNU General Public License.

[3] https://zenodo.org/badge/latestdoi/442700026
[4] https://github.com/rboston628/GRPulse

The code is being further developed in two directions. This present work highlights `GRPulse`'s capabilities for Newtonian and 1PN asteroseismology on simple models. `GRPulse` is also capable of calculating frequencies in the GR Cowling approximation, and we anticipate further developing its abilities to the full GR mode equations of Thorne & Campolattaro (1967) and Detweiler & Lindblom (1985). We have also extended the range of Newtonian stellar models to include more realistic models of WDs beyond polytropes, which we will present in a future study. We anticipate further expanding the number of models available in each regime of physics.

5.2. Polytropic Background Codes

We calculate the Newtonian polytropic background by numerically solving Equation (5) with simple RK4 on a uniform grid of fixed size $N_{\rm star}$. For $n = 0$, 1, and 5 there exist analytic solutions to test against (see Hansen & Kawaler 1994, Section 7.2). For a grid size $N_{\rm star} = 10^5$, we find relative errors from the analytic solutions always smaller than 10^{-13}. In addition, we can convert our solution to Equation (5) in terms of s and θ to a solution in terms of physical variables, such as r, ρ, P, and Φ, and insert these variables back into the original Equation (2) to calculate a scaled residual, e.g., for Equation (2a),

$$\mathrm{res}(r) = \frac{\left|\frac{d}{dr}\left(r^2\frac{d\Phi}{dr}\right) - 4\pi G\rho r^2\right|}{\left|\frac{d}{dr}\left(r^2\frac{d\Phi}{dr}\right)\right| + |4\pi G\rho r^2|}. \quad (52)$$

Across a range of indices n, and for $N_{\rm star} = 10^5$, we find this residual to be on the order 10^{-12}. We can define an rms residual (RMSR):

$$\mathrm{RMSR} = \sqrt{\frac{1}{R}\int_0^R \mathrm{res}^2(r)dr}, \quad (53)$$

which gives an estimate of numerical error. We can similarly define an RMSR for the eigenmodes by defining an analog to Equation (52) for Equation (8). If the RMSR is significantly smaller than the relative difference of the frequencies, we can be confident the difference is not due to numerical limitations in the calculation.

We calculate the 1PN polytropic background using an identical method, but where the parameter σ appearing in Equation (28) must also be fixed to match the surface redshift $z = \frac{GM}{c^2R}$. There are no known solutions to the 1PN polytrope equations, so no exact test can be performed. Tests of the residuals in the original Equation (24) are on the order 10^{-12} for $N_{\rm star} = 10^5$, across a range of n.

An additional test of the 1PN polytrope is to calculate overlap coefficients with both the Newtonian (0PN) and GR polytropic solutions, where the overlap is defined by

$$o(1, 2) = 1 - \frac{\langle\theta_1\theta_2\rangle}{\sqrt{\langle\theta_1\theta_1\rangle\langle\theta_2\theta_2\rangle}}, \quad (54)$$

with $\langle\theta_1\theta_2\rangle$ being the usual inner product of functions. The equation for a GR polytrope is a solution to the TOV equations with a polytropic equation of state and has been explored in depth elsewhere (Tooper 1964, 1965; Bludman 1973). It is expected that $\theta_{\rm 1pn}$ differs from $\theta_{\rm 0pn}$ by an amount that scales

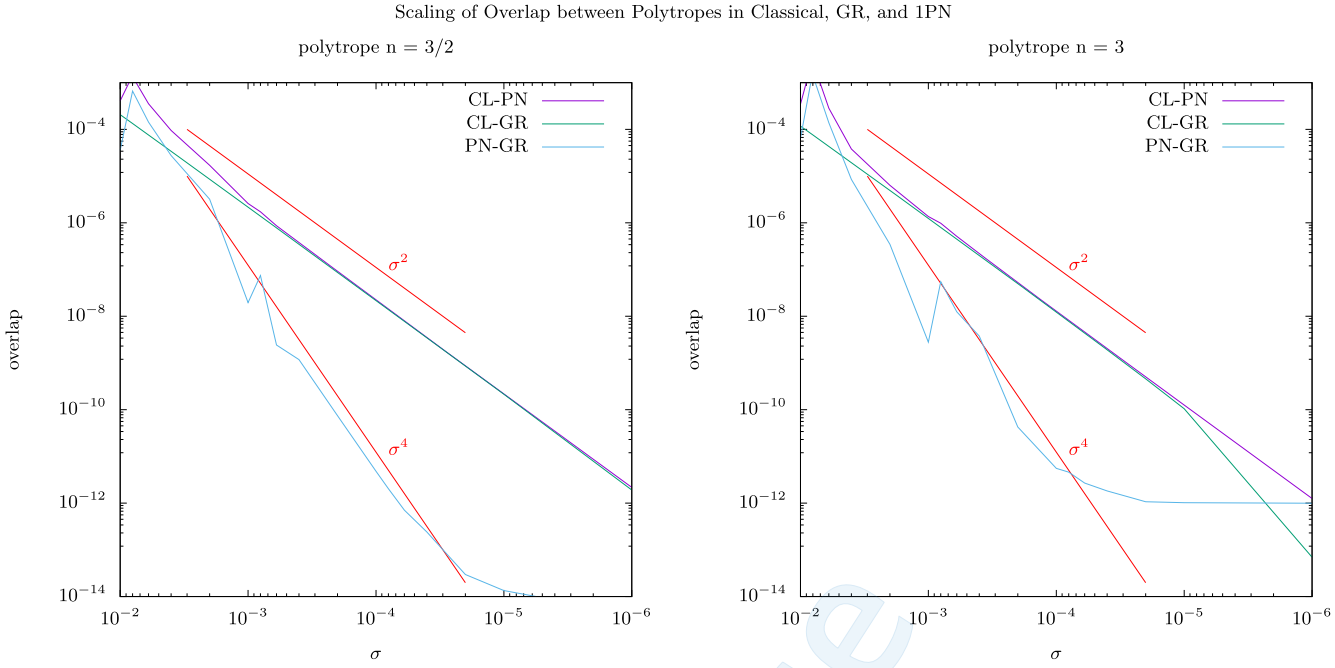

Figure 2. Convergence of 1PN and GR models to Newtonian as $\sigma \to 0$. The 1PN and GR models converge to the Newtonian model like σ^2, but converge to each other like σ^4. Shown for $n = 3/2$ (left) and $n = 3$ (right).

with σ defined in Equation (26), and that, therefore, $o(0\text{pn}, 1\text{pn}) \sim \sigma^2$. Similarly, $o(0\text{pn}, \text{GR}) \sim \sigma^2$, whereas $o(1\text{pn}, \text{GR}) \sim \sigma^4$. When both the 1PN and GR solutions are matched to Schwarzschild coordinates and compared, we find the expected scaling in σ for the overlaps, confirming that our 1PN polytrope accounts for GR up to order σ, with additional effects at order σ^2 (see Figure 2).

5.3. CHWD++ Background Codes

We calculate the Newtonian and 1PN CHWD++ background as above for the polytropes, using simple RK4 on a fixed grid of size N_{star}. There are no exact solutions to compare against, though we can compare the mass–radius relation of these models to the mass–radius relationship of real WDs. Tests of the residual in (2) and (24) are on the order 10^{-12} for $N_{\text{star}} = 10^5$.

5.4. Newtonian Stellar Pulsation Code

As with the background, we solve the pulsation equations using simple RK4 on a fixed, uniform grid. We choose the grid for pulsations to be $N_{\text{osc}} = \frac{1}{2}N_{\text{star}}$ so that the calculated background values can be used in the half-steps of the RK4 method without interpolation. The solution is found using a method similar to Christensen-Dalsgaard (2008). We shoot from both the center and the surface to an internal fitting position x_{fit}. At each boundary two independent solutions can be formed by choices of y_1 and y_3 in Equations (42) and (42b). The frequency $\bar{\omega}$ is adjusted to cause the two inward and two outward solutions to match, as determined by the vanishing of the Wronskian of the four solutions at x_{fit}. The physical solution is then made by a linear combination of the four solutions.

The resulting eigenmode is classified using the Osaki–Scuflaire method to identify mode order k for p- and g-modes. This method counts the mode order by the zero-crossings on a graph of y_1 and y_2, with clockwise crossings counted as negative. Positive mode orders are considered p-modes, and negative are g-modes.

In the case of an $n = 0$ polytrope (i.e., a uniform density star), there is an exact formula for the Newtonian eigenfrequencies of p-modes due to Pekeris (1938):

$$\bar{\omega}^2_{k\ell} = D_{k\ell} + \sqrt{D^2_{k\ell} + \ell(\ell+1)}\,, \tag{55}$$

where (JCD–DJM, Equation (3.3))

$$D_{k\ell} = \Gamma_1 k\left(k + \ell + \frac{1}{2}\right) - 2. \tag{56}$$

Here $k = 0, 1, 2, \ldots$ is the mode number, which counts radial nodes. An equivalent form of this equation is found in (Cox 1980, Equation (17).76), where $n = 0, 1, 2, \ldots$ is a recursion relation index, and is matched to mode number by $n = k - 1$. In the original of Pekeris (1938, Equation (32)), n corresponds to ℓ, and $k = 0, 2, 4, \ldots$ is another recursion relation index, which corresponds to $2n$ as found in Cox (1980). The uniform density model allows us to check the scaling of errors with N_{star} and with the mode order k. The results are shown in Figure 3.

We may also compare against the compiled tables of JCD–DJM, which are listed for p-modes to eight digits. To make this comparison, we multiply $\bar{\omega}$ by their scaling factor $\nu_g = 99.855377\,\mu$Hz. When compared to JCD–DJM, we almost always find either no difference or a difference of exactly $10^{-4}\mu$ Hz (i.e., at the least significant digit). The only exceptions occur due to an apparent difference in mode labeling in the low-order dipole ($\ell = 1$) p-modes of the $n = 4$ polytrope. This is due to the breakdown of the Osaki–Scuflaire method for classifying low-order dipole modes in centrally condensed stars, as discussed in Takata (2005; see Table 2). Correcting the labeling for the $k = 1, 2, 3, 4$, and 5 p-modes, we again find agreement with JCD–DJM to all digits in the $n = 4$ polytrope.

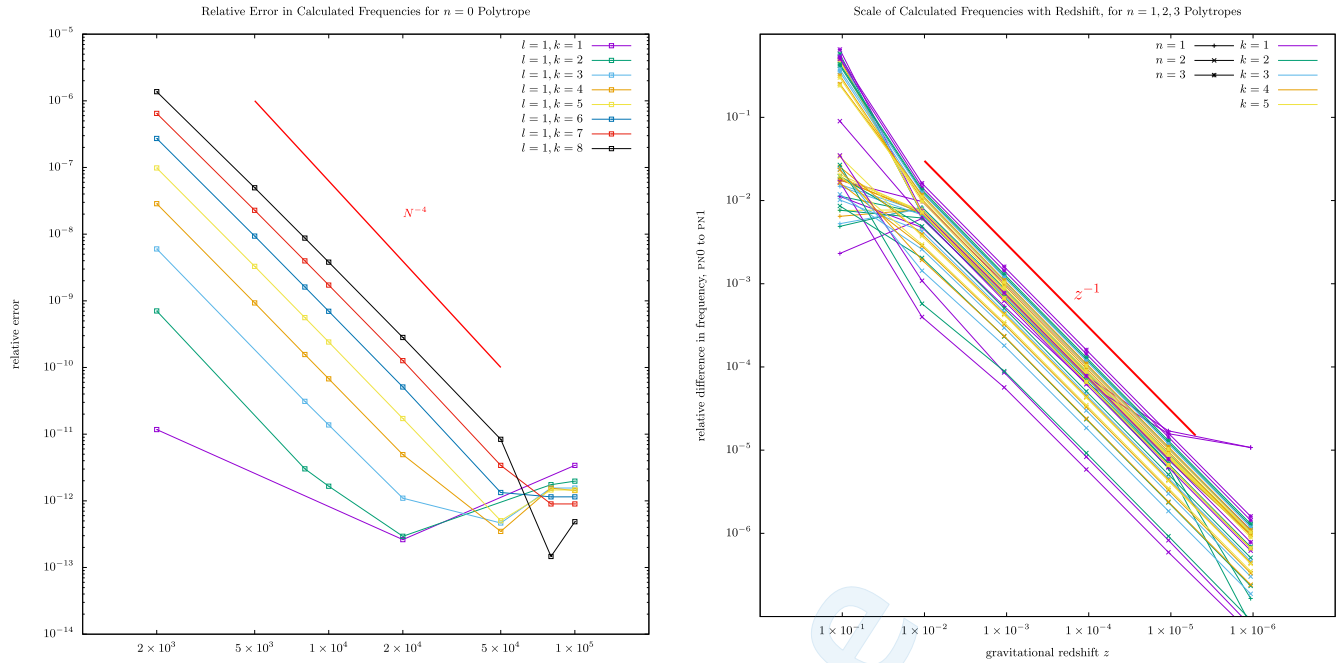

Figure 3. Left: the scaling of mode errors for $\ell = 1$ modes calculated against Equation (55) in an $n = 0$ polytrope. The errors scale like N^{-4}, and tend to increase for increasing k. Right: the scaling of differences between Newtonian and 1PN models for a range of redshifts z. Several polytropes were used with $\ell = 1 - 3$ and $k = 1 - 5$.

Table 1
Comparison of Fundamental Frequencies for Corresponding Newtonian 1PN Models with Cutler & Lindblom (1992)

	Newtonian			Post-Newtonian, $z = 0.2256$			
ℓ	$\bar{\omega}_{2022}$	$\bar{\omega}_{1992}$	% Err.	$\bar{\omega}_{2022}$	RMSR	$\bar{\omega}_{1992}$	Rel. Diff.
2	1.227	1.226	0.05%	1.317	0.07	1.232	0.06
3	1.698	1.697	0.05%	1.694	0.06	1.606	0.05
4	2.037	2.036	0.03%	1.984	0.05	1.885	0.05
5	2.310	2.309	0.03%	2.228	0.05	2.120	0.05
6	2.546	2.545	0.02%	2.444	0.04	2.324	0.05

Note. Mass and radius as in their Table 1. All models are a polytrope with $n = 1$ and $P \sim \rho^2 = (\epsilon/c)^2$, $\Gamma_1 = 1 + 1/n$.

Table 2
Comparison of Fundamental Frequencies for Corresponding 1PN GR Models with Lindblom et al. (1997)

	Post-Newtonian, $z = 0.1836$				General Relativity	
ℓ	$\bar{\omega}_{2022}$	RMSR	$\bar{\omega}_{1997}$	Rel. Diff.	$\bar{\omega}_{1997}$	Rel. Diff.
2	1.279	0.05	1.231	0.04	1.201	0.06
3	1.687	0.05	1.619	0.04	1.586	0.06
4	1.989	0.04	1.907	0.04	1.874	0.06
5	2.240	0.04	2.147	0.04	2.113	0.06

Note. Mass and radius as in their Table 1. All models are a polytrope with $n = 1$ and $P \sim \rho^2 = (\epsilon/c)^2$, $\Gamma_1 = 1 + 1/n$.

As with the background, the eigenfunctions, which are written in terms of the y_i variables, can be converted into a solution in terms of ΔP, ξ, etc., and inserted into Equation (8) to calculate an RMSR as in Equation (53). This residual is displayed in the tables in Section 6.

5.5. 1PN Stellar Pulsation Code

The same double-shooting RK4 method is used to solve the 1PN pulsation equations. Because there are eight equations, there are two additional solutions at both the center and surface and the Wronskian is the determinant of an 8×8 matrix instead of a 4×4. Otherwise, the 1PN eigenmodes are found in an identical manner to the Newtonian case. The eigenmode is also classified using the Osaki–Scuflaire method, again by counting crossings in y_1 and y_2, defined as in the 1PN approximation. For the 1PN case, the only error measurement we can use is the residual in the original physical equation. Due to mathematical manipulations truncating at first order in z, this residual scales with z^2, and for $z \sim 10^{-4}$, the residual should be $\sim 10^{-8}$. Because we are using identical numerical methods that we have verified in the Newtonian code, we can have additional confidence in the accuracy of the results.

There are no known analytic solutions for the 1PN frequencies. We do have a small table of f-mode frequencies to compare against, due to Cutler & Lindblom (1992; their Table 1), based on early work on the topic of 1PN oscillations in rotating neutron stars. They model the neutron star as an $n = 1$ polytrope, and list frequencies for $\ell = 2$ to 6 calculated using $\Gamma_1 = 1 + 1/n$. For the Newtonian star, they use $M = 1.736 M_\odot$ and $R = 15.343$ km, and for the 1PN star they use $M = 1.4 M_\odot$ and $R = 12.374$ km, which both give $z = 0.2256$. Their definition of the dimensionless frequency listed in their Table 1 differs from $\bar{\omega}$, defined in Equation (40) by $\bar{\omega}_{\rm CL} = \bar{\omega}\sqrt{4/3}$. Accounting for this difference, we find our numbers compare to theirs, as in Table 1. There is very close agreement on the Newtonian frequencies, and for the 1PN frequencies, differences are on the same order as the expected errors, $z^2 \sim 0.05$, which account for methodological differences made in the 1PN approximation.

There is a similar table in Lindblom et al. (1997; their Table 1), with $M = 1.4 M_\odot$ and $R = 14.45$ km, that lists both 1PN

Table 3
Normal Mode Frequencies and Periods for $n = 1.5$ Polytrope

	Newtonian Polytrope (RMSR $= 2 \times 10^{-12}$)				Post-Newtonian Polytrope (RMSR $= 2 \times 10^{-12}$)				$z \sim 10^{-4}$
l, k	$\bar{\omega}$	f (Hz)	Π (s)	RMSR	$\bar{\omega}$	f (Hz)	Π (s)	RMSR	Rel. Diff.
1, 1	2.571761	0.153246	6.525466	4×10^{-9}	2.571531	0.153207	6.527097	6×10^{-8}	-9.0×10^{-5}
1, 2	4.256099	0.253612	3.943034	4×10^{-9}	4.255778	0.253552	3.943964	7×10^{-8}	-7.5×10^{-5}
1, 3	5.838061	0.347878	2.874575	4×10^{-9}	5.837646	0.347797	2.875240	7×10^{-8}	-7.1×10^{-5}
1, 4	7.373488	0.439370	2.275984	4×10^{-9}	7.372978	0.439269	2.276507	7×10^{-8}	-6.9×10^{-5}
1, 5	8.881992	0.529259	1.889435	4×10^{-9}	8.881386	0.529138	1.889867	7×10^{-8}	-6.8×10^{-5}
1, 10	16.248203	0.968196	1.032849	4×10^{-9}	16.247119	0.967976	1.033084	7×10^{-8}	-6.7×10^{-5}
1, 15	23.505846	1.400663	0.713948	4×10^{-9}	23.504284	1.400345	0.714110	7×10^{-8}	-6.6×10^{-5}
1, 20	30.727923	1.831011	0.546146	4×10^{-9}	30.725885	1.830596	0.546270	7×10^{-8}	-6.6×10^{-5}
2, 0	1.455807	0.086748	11.527589	4×10^{-3}	1.455893	0.086740	11.528757	6×10^{-8}	-5.9×10^{-5}
2, 1	3.207357	0.191120	5.232327	3×10^{-9}	3.207218	0.191081	5.233395	6×10^{-8}	-4.3×10^{-5}
2, 2	4.849223	0.288955	3.460748	4×10^{-9}	4.848949	0.288892	3.461499	6×10^{-8}	-5.6×10^{-5}
2, 3	6.426896	0.382965	2.611205	4×10^{-9}	6.426508	0.382880	2.611782	7×10^{-8}	-6.0×10^{-5}
2, 4	7.966983	0.474735	2.106436	4×10^{-9}	7.966488	0.474630	2.106905	7×10^{-8}	-6.2×10^{-5}
2, 5	9.482660	0.565051	1.769750	4×10^{-9}	9.482060	0.564925	1.770146	7×10^{-8}	-6.3×10^{-5}
2, 10	16.882254	1.005977	0.994058	4×10^{-9}	16.881155	1.005750	0.994282	7×10^{-8}	-6.5×10^{-5}
2, 15	24.160416	1.439668	0.694605	4×10^{-9}	24.158830	1.439342	0.694762	7×10^{-8}	-6.6×10^{-5}
2, 20	31.395293	1.870778	0.534537	4×10^{-9}	31.393225	1.870355	0.534658	7×10^{-8}	-6.6×10^{-5}
3, 0	1.93432779	0.11526246	8.67585175	5×10^{-3}	1.93436853	0.11524638	8.67706176	5×10^{-8}	-2.1×10^{-5}
3, 1	3.695765	0.220223	4.540858	3×10^{-9}	3.695660	0.220181	4.541716	5×10^{-8}	-2.8×10^{-5}
3, 2	5.348647	0.318714	3.137605	4×10^{-9}	5.348409	0.318649	3.138248	6×10^{-8}	-4.5×10^{-5}
3, 3	6.941521	0.413630	2.417617	4×10^{-9}	6.941161	0.413543	2.418132	6×10^{-8}	-5.2×10^{-5}
3, 4	8.496828	0.506308	1.975083	4×10^{-9}	8.496354	0.506198	1.975510	6×10^{-8}	-5.6×10^{-5}
3, 5	10.026632	0.597466	1.673737	4×10^{-9}	10.026048	0.597335	1.674103	6×10^{-8}	-5.8×10^{-5}
3, 10	17.477641	1.041455	0.960195	4×10^{-9}	17.476538	1.041222	0.96042-	7×10^{-8}	-6.3×10^{-5}
3, 15	24.785387	1.476908	0.677090	4×10^{-9}	24.783786	1.476576	0.677243	7×10^{-8}	-6.5×10^{-5}
3, 20	32.038738	1.909120	0.523802	4×10^{-9}	32.036649	1.908689	0.523920	7×10^{-8}	-6.5×10^{-5}

Note. Both stars are scaled to $M = 0.6 M_\odot$ and $R = 1.3 R_\oplus$. All modes use $\Gamma_1 = 5/3$. There are no g-modes for this model.

frequencies and GR frequencies for the same star. We find similar agreement with both sets of numbers, shown in Table 2.

The 1PN approximation is not ideal for a highly compact object such as a neutron star, unless numerical errors as high as 5% are acceptable. For a WD, the systemic errors in using the 1PN approximation are orders of magnitude smaller.

6. Results

For the following calculations we model polytropes, scaled so that the total mass equals a typical field WD mass of $M = 0.6 M_\odot$ (or $M = 1.1934 \times 10^{33}$ g), with $R = 1.3 R_\oplus$ (or $R = 8282$ km). The radius is picked based on models of the WD mass–radius relationship. There is an important subtlety here in how we choose background WD models in order to compare Newtonian and 1PN mode periods. We consider the mass of the stars first. For a Newtonian polytrope, the meaning of mass is clear. When considering GR, the observed mass of a WD is the gravitational mass M, which is a combination of the integrated baryon mass, internal energy, and gravitational binding energy. When we compare a Newtonian WD to a 1PN WD, we keep the mass M fixed.

For a Newtonian polytrope, the natural second parameter needed to specify the star is the radius, R, which is unambiguously defined. Other quantities that are combinations of M and R might be used in place of R in order to define the polytrope. In GR, there is, however, a coordinate ambiguity in defining the radius of a star. Our equations for the static background model are written in terms of an isotropic radial coordinate $r = r_{\rm i}$, which appears when we convert the background line element (Equation (18)) into spherical coordinates:

$$ds^2 = -\left(1 + \frac{2\Phi}{c^2} + \frac{2(\Psi + \Phi^2)}{c^4}\right)c^2 dt^2 + \left(1 - \frac{2\Phi}{c^2}\right)(dr_{\rm i}^2 + r_{\rm i}^2 d\Omega^2). \quad (57)$$

However, the radius of an isolated real WD can be indirectly estimated from observables such as the surface gravitational redshift z or the surface gravity g_s, determined by spectal line shifts and broadening, respectively. For a spherical WD background, the exterior region, which connects the surface properties to a distant observer, is described by the Schwarzschild solution. In standard Schwarzschild coordinates it has a line element given by

$$ds^2 = -\left(1 - \frac{2GM}{c^2 r_{\rm a}}\right)c^2\, dt^2 + \left(1 - \frac{2GM}{c^2 r_{\rm a}}\right)^{-1} dr_{\rm a}^2 + r_{\rm a}^2\, d\Omega^2, \quad (58)$$

where $r_{\rm a}$ is the areal radial coordinate. Any calculation of the radius from surface redshift $z = GM/(c^2 R)$ (or from the surface gravity) will give a value for $R = R_{\rm a}$ in this latter coordinate system. We make the choice that the radius we specify based on the mass–radius relation is the areal radius $R_{\rm a}$. On the other hand, the background star might be described in terms of

Table 4
Normal Mode Frequencies and Periods for $n = 3$ Polytrope

	Newtonian Polytrope (RMSR $= 2 \times 10^{-12}$)				Post-Newtonian Polytrope (RMSR $= 2 \times 10^{-12}$)				$z \sim 10^{-4}$
l, k	$\bar{\omega}$	f (Hz)	Π (s)	RMSR	$\bar{\omega}$	f (Hz)	Π (s)	RMSR	Rel. Diff.
1, −10	0.343611	0.020475	48.839961	9×10^{-12}	0.343666	0.020475	48.839927	4×10^{-7}	1.6×10^{-4}
1, −5	0.608215	0.036242	27.592119	3×10^{-12}	0.608315	0.036242	27.592025	4×10^{-7}	1.6×10^{-4}
1, −4	0.719567	0.042877	23.322293	3×10^{-12}	0.719686	0.042878	23.322150	4×10^{-7}	1.7×10^{-4}
1, −3	0.880757	0.052482	19.053998	2×10^{-12}	0.880909	0.052483	19.053777	3×10^{-7}	1.7×10^{-4}
1, −2	1.133891	0.067566	14.800318	2×10^{-12}	1.134099	0.067568	14.799968	3×10^{-7}	1.8×10^{-4}
1, −1	1.586168	0.094516	10.580181	1×10^{-12}	1.586506	0.094521	10.579625	2×10^{-7}	2.1×10^{-4}
1, 1	3.377036	0.201230	4.969429	1×10^{-12}	3.377300	0.201214	4.969838	2×10^{-7}	7.8×10^{-5}
1, 2	4.642432	0.276633	3.614903	2×10^{-12}	4.642751	0.276607	3.615235	2×10^{-7}	6.9×10^{-5}
1, 3	5.909240	0.352119	2.839949	2×10^{-12}	5.909632	0.352086	2.840217	2×10^{-7}	6.6×10^{-5}
1, 4	7.176668	0.427642	2.338403	2×10^{-12}	7.177142	0.427602	2.338624	2×10^{-7}	6.6×10^{-5}
1, 5	8.443277	0.503117	1.987610	2×10^{-12}	8.443837	0.503069	1.987797	2×10^{-7}	6.6×10^{-5}
1, 10	14.751133	0.878988	1.137671	1×10^{-11}	14.752152	0.878908	1.137775	2×10^{-7}	6.9×10^{-5}
2, −10	0.567887	0.033839	29.551565	2×10^{-11}	0.567978	0.033839	29.551593	4×10^{-7}	1.6×10^{-4}
2, −5	0.967663	0.057661	17.342746	4×10^{-12}	0.967817	0.057661	17.342780	4×10^{-7}	1.6×10^{-4}
2, −4	1.127173	0.067166	14.888523	4×10^{-12}	1.127352	0.067166	14.888544	4×10^{-7}	1.6×10^{-4}
2, −3	1.349915	0.080439	12.431848	2×10^{-12}	1.350133	0.080439	12.431843	3×10^{-7}	1.6×10^{-4}
2, −2	1.681711	0.100210	9.979088	2×10^{-12}	1.681991	0.100210	9.979029	3×10^{-7}	1.7×10^{-4}
2, −1	2.216884	0.132099	7.570059	2×10^{-12}	2.217291	0.132102	7.569883	3×10^{-7}	1.8×10^{-4}
2, 0	2.859255	0.170377	5.869340	1×10^{-12}	2.859867	0.170386	5.869026	2×10^{-7}	2.1×10^{-4}
2, 1	3.906874	0.232802	4.295491	1×10^{-12}	3.907499	0.232802	4.295493	2×10^{-7}	1.6×10^{-4}
2, 2	5.169469	0.308038	3.246357	1×10^{-12}	5.170107	0.308026	3.246478	2×10^{-7}	1.2×10^{-4}
2, 3	6.439990	0.383745	2.605895	2×10^{-12}	6.440673	0.383724	2.606037	2×10^{-7}	1.1×10^{-4}
2, 4	7.708951	0.459360	2.176942	2×10^{-12}	7.709691	0.459330	2.177083	2×10^{-7}	9.6×10^{-5}
2, 5	8.975891	0.534854	1.869668	2×10^{-12}	8.976697	0.534816	1.869802	2×10^{-7}	9.0×10^{-5}
2, 10	15.284901	0.910795	1.097942	2×10^{-11}	15.286091	0.910719	1.098033	2×10^{-7}	7.8×10^{-5}
3, −10	0.766497	0.045674	21.894321	2×10^{-11}	0.766618	0.045674	21.894388	4×10^{-7}	1.6×10^{-4}
3, −5	1.259737	0.075065	13.321780	5×10^{-12}	1.259929	0.075064	13.321887	4×10^{-7}	1.5×10^{-4}
3, −4	1.446622	0.086201	11.600779	9×10^{-12}	1.446840	0.086200	11.600890	4×10^{-7}	1.5×10^{-4}
3, −3	1.699020	0.101241	9.877421	4×10^{-12}	1.699274	0.101240	9.877531	3×10^{-7}	1.5×10^{-4}
3, −2	2.058262	0.122647	8.153451	2×10^{-12}	2.058568	0.122646	8.153550	3×10^{-7}	1.5×10^{-4}
3, −1	2.601340	0.155008	6.451267	2×10^{-12}	2.601732	0.155007	6.451330	3×10^{-7}	1.5×10^{-4}
3, 0	3.068190	0.182827	5.469654	2×10^{-12}	3.068607	0.182822	5.469790	3×10^{-7}	1.4×10^{-4}
3, 1	4.294602	0.255906	3.907682	2×10^{-12}	4.295218	0.255902	3.907750	2×10^{-7}	1.4×10^{-4}
3, 2	5.591067	0.333160	3.001563	2×10^{-12}	5.591792	0.333149	3.001656	2×10^{-7}	1.3×10^{-4}
3, 3	6.878680	0.409886	2.439704	2×10^{-12}	6.879493	0.409869	2.439807	2×10^{-7}	1.2×10^{-4}
3, 4	8.158826	0.486167	2.056906	2×10^{-12}	8.159719	0.486142	2.057011	2×10^{-7}	1.1×10^{-4}
3, 5	9.433911	0.562147	1.778895	3×10^{-12}	9.434880	0.562114	1.778998	2×10^{-7}	1.0×10^{-4}
3, 10	15.767068	0.939526	1.064367	2×10^{-11}	15.768422	0.939456	1.064446	2×10^{-7}	8.6×10^{-5}

Note. Both stars are scaled to $M = 0.6 M_\odot$ and $R = 1.3 R_\oplus$. All modes use $\Gamma_1 = 5/3$.

isotropic coordinates, in which case its radius would be R_i, differing at 1PN order from R_a. These two radii can be related by

$$R_\mathrm{a} = R_\mathrm{i}\sqrt{1 - \frac{2GM}{c^2 R_\mathrm{i}}}. \tag{59}$$

Given our choice for mass M and radius R_a, we might alternatively view the surface redshift $z = GM/(c^2 R_\mathrm{a}) = 1.07 \times 10^{-4}$ as the second polytropic parameter to hold fixed in comparing Newtonian and 1PN models. We adopt these values as parameters in our subsequent polytrope calculations.

In Tables 3 and 4, we compile eigenfrequencies calculated on $n = 1.5$ and $n = 3$ polytrope backgrounds. The table records the dimensionless frequency $\bar{\omega}$, the cyclic frequency f (in hertz), the period Π (in seconds), and the RMSR. In an additional column, we specify the relative difference between $\bar{\omega}$ in the Newtonian and 1PN calculations, defined in the sense

$$\text{rel. diff.} = \frac{\bar{\omega}_{1\mathrm{pn}} - \bar{\omega}_{0\mathrm{pn}}}{\bar{\omega}_{\mathrm{avg}}}, \tag{60}$$

àso that a positive relative difference means the 1PN frequency is blueshifted, while a negative difference means redshifted. The differences between periods are similar to those between $\bar{\omega}$. The RMSR for the stars and modes is as defined in Equation (53). Additional tables for several values of n can be found in Boston (2022).

Note that g-modes are unstable for $n \leqslant 1.5$ and that there is no f-mode ($k = 0$) for $\ell = 1$.

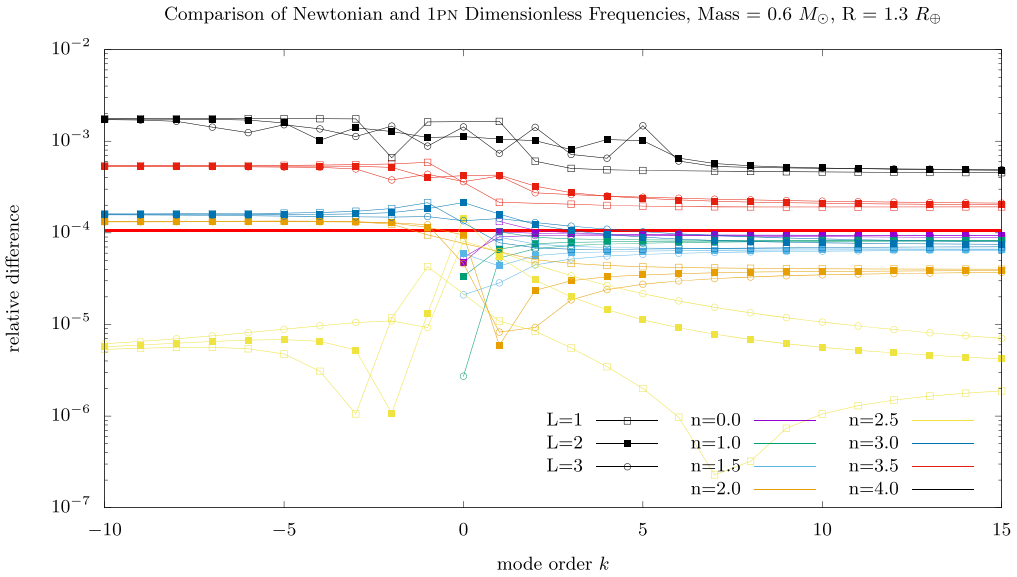

Figure 4. Graph of relative differences in $\bar{\omega}$ between models for several polytrope models. The central red line shows $z = 1.07 \times 10^{-4}$. The dependence on mode type (g- or p-modes) and the dependence on model is evident from the graph. Of particular interest is $n = 2.5$, where the difference between Newtonian and 1PN frequencies becomes much smaller than z, or for $n > 3$, where the difference becomes much larger than z.

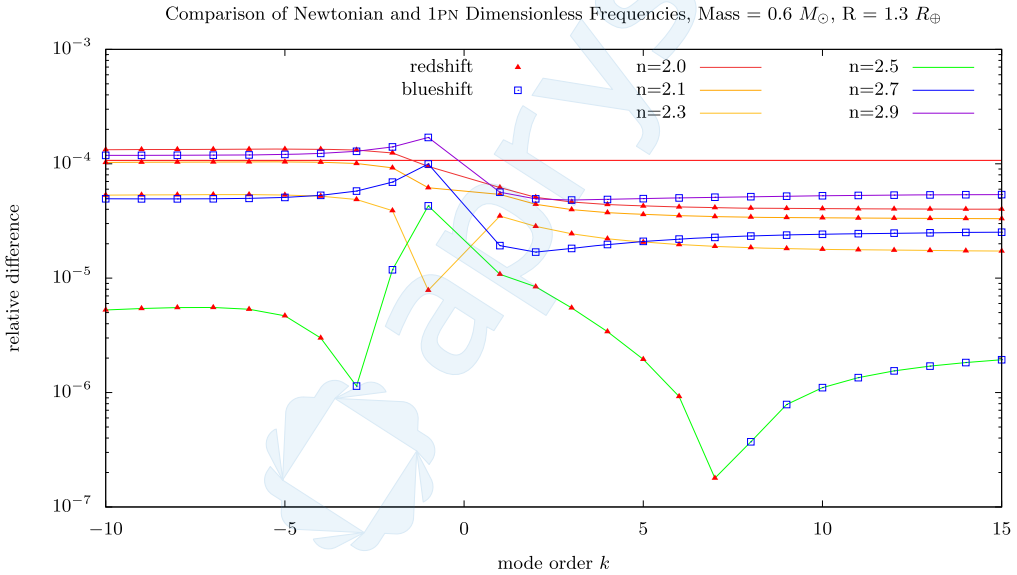

Figure 5. Refined graph for many models in the range $n \in [2, 3]$, arranged in rough chromatic order with increasing n, with $\ell = 1$ for all modes. Frequencies with a positive difference (meaning $\bar{\omega}_{1\mathrm{pn}}$ has been blueshifted) and frequencies with a negative difference (meaning $\bar{\omega}_{1\mathrm{pn}}$ has been redshifted) are marked with different symbols. The sign shift occurs between $n = 2.5$ and $n = 2.7$, suggesting the existence of a polytropic index where the difference will be zero for some modes.

Results for many more polytrope models are graphed in Figure 4. A careful look at the tables will reveal that between $n = 1.5$ and $n = 3$ the frequencies change from redshifted to blueshifted. In Figure 5 more results are graphed in the range $n = 2$ to $n = 3$, showing this shift occurs around $n = 2.6$.

For the CHWD++ models, the choice of y_0 fixes M and R according to a mass–radius relation, and therefore it is not possible to freely scale z to match between the Newtonian and 1PN models. We therefore choose to match them according to M. In Table 5, we list eigenfrequencies calculated on a CHWD ++ background matched to $M = 0.607158 M_\odot$. This table records the dimensionless frequency $\bar{\omega}$, the period Π (in seconds), and the RMSR, along with the relative difference, as in Equation (60).

7. Discussion

The results presented in Section 6 generally confirm that GR will lead to measurable changes at the 1PN level in periods derived from space-based photometry for compact stellar objects of similar mass and radius as WDs. This change, represented by the relative difference, is roughly of the same order of magnitude as the gravitational surface redshift z. Because the effect is measurable, the full precision of the photometric data from K2 and TESS cannot be used to fit asteroseismic models of stars unless GR is first included in both the model and perturbation equations. We recommend the 1PN formalism as the simplest way to do this, and our set of Equations (49a)–(49h) might conveniently be added to existing asteroseismology codes.

Table 5
Normal Mode Frequencies and Periods for a CHWD++ with $M = 0.60716 M_{\odot}$

	Newtonian CHWD++ (RMSR $= 1 \times 10^{-10}$)			Post-Newtonian CHWD++ (RMSR $= 3 \times 10^{-13}$)			
	$y_0 = 1.57991$, $z = 1.0301 \times 10^{-4}$			$y_0 = 1.581$, $z = 1.0317 \times 10^{-4}$			
l, k	$\bar{\omega}$	Π (s)	RMSR	$\bar{\omega}$	Π (s)	RMSR	Rel. Diff.
1, −8	0.0104963	1711.4055481	6×10^{-6}	0.0105004	1708.4024156	3×10^{-5}	3.87×10^{-4}
1, −7	0.0119985	1497.1386391	6×10^{-7}	0.0120032	1494.5113986	5×10^{-7}	3.87×10^{-4}
1, −6	0.0140044	1282.7042090	6×10^{-7}	0.0140098	1280.4531595	3×10^{-6}	3.87×10^{-4}
1, −5	0.0168196	1068.0042846	2×10^{-7}	0.0168261	1066.1299007	2×10^{-7}	3.87×10^{-4}
1, −4	0.0210630	852.8448434	1×10^{-7}	0.0210711	851.3479456	1×10^{-7}	3.87×10^{-4}
1, −3	0.0282100	636.7745033	4×10^{-8}	0.0282210	635.6567139	9×10^{-8}	3.88×10^{-4}
1, −2	0.0429319	418.4169279	1×10^{-8}	0.0429486	417.6823108	7×10^{-8}	3.88×10^{-4}
1, −1	0.0945682	189.9521474	1×10^{-8}	0.0946049	189.6186247	7×10^{-8}	3.88×10^{-4}
2, −8	0.0181734	988.4458576	2×10^{-6}	0.0181804	986.7117546	2×10^{-5}	3.87×10^{-4}
2, −7	0.0207742	864.6997279	6×10^{-7}	0.0207822	863.1826760	5×10^{-7}	3.87×10^{-4}
2, −6	0.0242469	740.8560180	6×10^{-7}	0.0242562	739.5561899	5×10^{-6}	3.87×10^{-4}
2, −5	0.0291209	616.8580678	2×10^{-7}	0.0291321	615.7757375	2×10^{-7}	3.87×10^{-4}
2, −4	0.0364670	492.5937394	2×10^{-7}	0.0364812	491.7293805	1×10^{-7}	3.87×10^{-4}
2, −3	0.0488399	367.8022592	4×10^{-8}	0.0488588	367.1568083	9×10^{-8}	3.87×10^{-4}
2, −2	0.0743247	241.6886386	2×10^{-8}	0.0743535	241.2644417	7×10^{-8}	3.87×10^{-4}
2, −1	0.1637001	109.7338397	1×10^{-8}	0.1637635	109.5412449	7×10^{-8}	3.87×10^{-4}
3, −8	0.0256886	699.2757612	1×10^{-6}	0.0256986	698.0493223	6×10^{-6}	3.86×10^{-4}
3, −7	0.0293645	611.7396636	8×10^{-7}	0.0293759	610.6667318	5×10^{-7}	3.86×10^{-4}
3, −6	0.0342726	524.1335104	5×10^{-7}	0.0342859	523.2142080	2×10^{-6}	3.86×10^{-4}
3, −5	0.0411612	436.4171049	2×10^{-7}	0.0411771	435.6516259	2×10^{-7}	3.86×10^{-4}
3, −4	0.0515434	348.5109838	3×10^{-7}	0.0515633	347.8996633	1×10^{-7}	3.86×10^{-4}
3, −3	0.0690290	260.2305123	4×10^{-8}	0.0690556	259.7740126	8×10^{-8}	3.86×10^{-4}
3, −2	0.1050413	171.0130636	2×10^{-8}	0.1050819	170.7130437	7×10^{-8}	3.87×10^{-4}
3, −1	0.2313130	77.6585806	1×10^{-8}	0.2314024	77.5223589	7×10^{-8}	3.86×10^{-4}

Note. All modes use Γ_1 calculated from the background equation of state.

The neglect of GR is not the largest source of error in normal mode calculations for WDs. Other factors besides 1PN gravitational fields, such as differences in the equation of state, composition, opacity, or treatment of convection, will have larger numerical impacts. Using the 1PN equations does not guarantee a full fit to the K2 and TESS data. However, our results indicate that the size of the 1PN correction is now observationally significant. One of the main purposes of asteroseismology is to solve the inverse problem, using observed mode periods to infer underlying stellar parameters, such as total mass, fractional composition, temperature, radius, rotation, existence of solid core, etc. Any purely Newtonian approach to model a pulsating WD, such as fitting eigenperiods to the full resolution of K2 or TESS, will give rise to errors in interpreted values of physical parameters at a fractional level of $\sim 10^{-4}$.

The results also show that the underlying stellar model is important in determining not only the extent that GR changes the frequency, but whether the frequencies are blue- or redshifted. The relative differences for polytropes undergo a sign change between $n = 2$ and $n = 3$, which suggests a balancing act of competing effects. For larger n, the mass of the star is more centrally condensed, causing β_*^2 to become distinctly larger than z in the center, driving up the difference. At the same time, with increasing n the star becomes more diffuse near the surface, and smaller densities lead to a smaller local strength of relativity in the outer layers, driving down the difference. Somewhere between $n = 2.5$ and $n = 2.7$, the diffuse atmosphere becomes the most important effect and the difference drops to nearly zero, whereas with further increasing n, the increasingly compact core becomes the more important effect.[5] Whether this same balancing act occurs in a real WD is a subject for future study, but the present work indicates that the GR correction in a real WD will not be as simple as merely gravitationally redshifting the frequencies.

Acknowledgments

We thank J. J. Hermes and Bart H. Dunlap for helpful discussions and pointing out several important observational results. This paper was partially supported by NSF grant Nos. PHY-1506182, PHY-1806447, and PHY-2110335, and the North Carolina Space Grant Graduate Research Fellowship through NASA. R.B. thanks his mother, father, and wife.

ORCID iDs

S. Reece Boston https://orcid.org/0000-0001-8122-1961
Charles R. Evans https://orcid.org/0000-0001-5578-1033
J. Christopher Clemens https://orcid.org/0000-0003-1964-2612

References

Althaus, L. G., Camisassa, M. E., Torres, S., et al. 2022, A&A, 668, A58
Arun, K. G., Blanchet, L., Iyer, B. R., & Qusailah, M. S. S. 2008, PhRvD, 77, 064034
Barrera, R. G., Estévez, G. A., & Giraldo, J. 1985, EJPh, 6, 287
Blanchet, L. 2014, LRR, 17, 2
Bludman, S. A. 1973, ApJ, 183, 637
Boston, S. R. 2022, PhD thesis, Univ. North Carolina
Brassard, P., Fontaine, G., Wesemael, F., et al. 1991, ApJ, 367, 601

[5] Our thanks to Kip Thorne for suggesting this possibility.

Brassard, P., Wesemael, F., & Fontaine, G. 1989, Second-Order Effects due to Rotation in Pulsating DA White Dwarfs, White Dwarfs , 328 (Lecture Notes in Physics) ed. G. Wegner, (Heidelberg: Springer), 258
Brickhill, A. J. 1991, MNRAS, 251, 673
Campolattaro, A., & Thorne, K. S. 1970, ApJ, 159, 847
Carvalho, G. A., Marinho, R. M., & Malheiro, M. 2018, GReGr, 50, 38
Chandrasekhar, S. 1939, An Introduction to the Study of Stellar Structure (Chicago: Univ. Chicago Press)
Chandrasekhar, S., & Tooper, R. F. 1964, ApJ, 139, 1396
Christensen-Dalsgaard, J. 2008, Ap&SS, 316, 113
Christensen-Dalsgaard, J., & Mullan, D. J. 1994, MNRAS, 270, 921
Córsico, A. H., & Benvenuto, O. G. 2002, Ap&SS, 279, 281
Cowling, T. G. 1941, MNRAS, 101, 367
Cox, J. P. 1980, Theory of Stellar Pulsation, Vol. 2 (Princeton, NJ: Princeton Univ. Press)
Cutler, C. 1991, ApJ, 374, 248
Cutler, C., & Lindblom, L. 1992, ApJ, 385, 630
Detweiler, S., & Lindblom, L. 1985, ApJ, 292, 12
Dolez, N., & Vauclair, G. 1981, A&A, 102, 375
Dziembowski, W. A. 1971, AcA, 21, 289
Finn, L. S. 1986, MNRAS, 222, 393
Finn, L. S. 1987, MNRAS, 227, 265
Finn, L. S. 1988, MNRAS, 232, 259
Giammichele, N., Charpinet, S., Fontaine, G., et al. 2018, Natur, 554, 73
Goldreich, P., & Wu, Y. 1999, ApJ, 511, 904
Hansen, C. J., & Kawaler, S. D. 1994, Stellar Interiors: Physical Principles, Structure, and Evolution (Berlin: Springer-Verlag)
Harrison, B. K., Thorne, K. S., Wakano, M., & Wheeler, J. A. 1965, Gravitation Theory and Gravitational Collapse
Hermes, J. J., Gänsicke, B. T., Kawaler, S. D., et al. 2017, ApJS, 232, 23
Hermes, J. J., Montgomery, M. H., Mullally, F., et al. 2013, ApJ, 766, 42
Ipser, J. R., & Thorne, K. S. 1973, ApJ, 181, 181
Kawaler, S. D., Winget, D. E., & Hansen, C. J. 1985, ApJ, 295, 547
Kepler, S. O., Robinson, E. L., & Nather, R. E. 1983, ApJ, 271, 744
Kepler, S. O., Winget, D. E., Vanderbosch, Z. P., et al. 2021, ApJ, 906, 7
Lane, H. J. 1870, AmJS, 50, 57
Lindblom, L., & Detweiler, S. L. 1983, ApJS, 53, 73
Lindblom, L., Mendell, G., & Ipser, J. R. 1997, PhRvD, 56, 2118
Lindblom, L., & Splinter, R. J. 1990, ApJ, 348, 198
Mathew, A., & Nandy, M. K. 2017, RAA, 17, 061
McDermott, P. N., Hansen, C. J., van Horn, H. M., & Buland, R. 1985, ApJL, 297, L37
McDermott, P. N., van Horn, H. M., & Scholl, J. F. 1983, ApJ, 268, 837
Mukadam, A. S., Bischoff-Kim, A., Fraser, O., et al. 2013, ApJ, 771, 17
Nunes, S. P., Arbañil, J. D. V., & Malheiro, M. 2021, ApJ, 921, 138
Odonoghue, D. E., & Warner, B. 1982, MNRAS, 200, 563
Oppenheimer, J. R., & Volkoff, G. M. 1939, PhRv, 55, 374
Osaki, Y. 1975, PASJ, 27, 237
Paxton, B., Bildsten, L., Dotter, A., et al. 2010, MESA: Modules for Experiments in Stellar Astrophysics, Astrophysics Source Code Library, ascl:http://ascl.net/1010.083
Pekeris, C. L. 1938, ApJ, 88, 189
Poisson, E., & Will, C. M. 2014, Gravity: Newtonian, Post-Newtonian, Relativistic (1st edn.; Cambridge: Cambridge Univ. Press)
Price, R., & Thorne, K. S. 1969, ApJ, 155, 163
Scuflaire, R. 1974, A&A, 36, 107
Shapiro, S. L., & Teukolsky, S. A. 1983, Black Holes, White Dwarfs, and Neutron Stars: the Physics of Compact Objects (New York: Wiley)
Takata, M. 2005, PASJ, 57, 375
Takata, M., & Löffler, W. 2004, PASJ, 56, 645
Thorne, K. S. 1969a, ApJ, 158, 1
Thorne, K. S. 1969b, ApJ, 158, 997
Thorne, K. S., & Campolattaro, A. 1967, ApJ, 149, 591
Tolman, R. C. 1939, PhRv, 55, 364
Tooper, R. F. 1964, ApJ, 140, 434
Tooper, R. F. 1965, ApJ, 142, 1541
Townsend, R. H. D., & Teitler, S. A. 2013, MNRAS, 435, 3406
Unno, W., Osaki, Y., Ando, H., & Shibahashi, H. 1979, Nonradial Oscillations of Stars (Tokyo: University of Tokyo Press)
Weinberg, S. 1972, Gravitation and Cosmology: Principles and Applications of the General Theory of Relativity (New York: Wiley)
Winget, D. E., van Horn, H. M., Tassoul, M., et al. 1982, ApJL, 252, L65
Wu, Y., & Goldreich, P. 2001, ApJ, 546, 469
Yoshida, S., & Lee, U. 2002, Astronomy and Astrophysics, 395, 201